International Journal of Materials Chemistry and Physics
Vol. 1, No. 1, 2015, pp. 43-66
http://www.aiscience.org/journal/ijmcp

Boride Coatings of Fe–Cr Alloys and Chromium Steels

V. I. Dybkov*

Department of Physical Chemistry of Inorganic Materials, Institute of Problems of Materials Science, National Academy of Sciences of Ukraine, Kyiv, Ukraine

Abstract

Boriding of Fe–Cr alloy (5-30% chromium) and commercial chromium steel (13 and 25% Cr) samples in amorphous boron powder at 850–950ºC and reaction times 3600-43200 s (1-12 h) results in the formation of a surface coating consisting of two boride layers. In the case of Fe–Cr alloys containing 5-15% chromium and a 13% Cr steel, the outer layer bordering the boriding agent consists of the (Fe,Cr)B phase, whereas the inner adjacent to the solid substrate consists of the (Fe,Cr)2B phase. Each layer is a homogeneous phase (microstructure of the first type). With Fe–Cr alloys containing 25 and 30% chromium and a 25% Cr steel, each of two boride layers consists of two phases. The outer layer comprises the (Fe,Cr)B and (Cr,Fe)B phases, while the inner comprises the (Fe,Cr)2B and (Cr,Fe)2B phases. Both layers have a regular network-platelet microstructure of the second type. With Fe–5% Cr and Fe–10% Cr alloys, boriding during 3600 s leads to the formation of a single (Fe,Cr)2B layer. The next (Fe,Cr)B layer occurs after the first-formed (Fe,Cr)2B layer has reached, depending on the temperature of reaction, a thickness of 100-180 μm. With other alloys and steels, a reaction time of 3600 s is sufficient for both boride layers (Fe,Cr)B and (Fe,Cr)2B to occur. The characteristic feature of the layers is a pronounced texture, the strongest reflections being {002} and {020} for the FeB phase and {002} for the Fe2B phase. Diffusional growth kinetics of boride layers are close to parabolic and can more adequately be described by a system of two non-linear differential equations. Values of layer growth-rate constants are provided. Their temperature dependence obeys a relation of the Arrhenius type. Boride layers with the microstructure of the second type exhibit a much higher wear resistance than those with the microstructure of the first type, the difference being more than an order of magnitude.

Keywords

Fe–Cr Alloys and Chromium Steels, Boride Coatings, Microstructure, Phase Identity, Chemical Composition, Microhardness, Dry Abrasive Wear Resistance

Received: May 29, 2015 / Accepted: June 14, 2015 / Published online: July 16, 2015

1. Introduction

Boriding is a kind of surface treatments aimed at improving service characteristics of products and parts from metals, alloys and steels [1–5]. It provides a high increase in their hardness and resistance to abrasion, wear and corrosion, with a negligible change in dimensions of the original part. A variety of borided parts are now routinely manufactured, from pipe fittings to critical aerospace components.

The phase diagram is the main source of preliminary information necessary in order to choose an optimum regime of the boriding procedure. Two iron borides FeB and Fe2B are known to exist in the Fe–B binary system [6–8]. With iron, its alloys and low-alloy steels, one (either FeB or Fe2B) or two (both FeB and Fe2B) boride phases can therefore form as separate continuous layers in a coating on the surface of a solid substrate, depending on boriding agents and temperature-time conditions employed.

* Corresponding author
E-mail address: vdybkov@ukr.net, vdybkov@ipms. kiev.ua

Physical, chemical and mechanical properties of boride layers are known to be rather sensitive to the amount of alloying elements and impurities present in a base material. In the case of materials of complicated chemical composition such as multi-component alloys and steels, with which the vast majority of experiments have hitherto been carried out (see, for example, [9-18]), it is not always easy to separate the effect of a particular element on those properties from that of others. To facilitate this task, experiments with binary iron-base alloys are therefore badly needed.

In this work, experimental data [19–28] on the interaction of five iron-chromium alloys (5, 10, 15, 25 and 30% Cr) and two commercial steels containing 13 and 25% Cr with boron in a mixture of amorphous boron powder and KBF4 (activator) in the temperature range of 850–950oC at reaction times up to 43200 s (12 h) are presented in a systematic way and discussed from a single theoretical viewpoint. First of all, attention is paid to the phase identification of boride layers formed at the interface of a solid alloy or steel sample with boron and the determination of their chemical composition. Then, mechanism of layer formation is considered in detail from a chemical viewpoint to provide evidence for the inadequacy of some too simplified physical and metallurgical imaginations existing in the available literature. Besides, mathematical equations describing layer-growth kinetics and taking account of the rate of chemical transformations at the layer interfaces and the rate of diffusion across their bulks are briefly analyzed to show why in many cases the solid-state growth of compound layers is neither simultaneous, nor parabolic, as follows from purely diffusional considerations. Eventually, interconnection between the structure and mechanical properties, notably microhardness and dry abrasive wear resistance of boride coatings formed on the surface of alloy or steel samples, is demonstrated.

2. Experimental

2.1. Materials and Samples

The materials used for the preparation of iron-chromium alloys included carbonyl iron powder (99.98% Fe) and electrolytic-grade chromium platelets (99.98% Cr). All contents are given in mass percent if otherwise not stated. Reagents were amorphous boron powder and analytical-grade KBF_4.

Cylindrical rods of Fe–Cr alloys (5, 10, 15, 25 and 30% chromium) were prepared by arc-melting of appropriate amounts of metals under argon, with subsequent casting of the melts into water-cooled copper crucibles. The rods were annealed at a temperature of 1100°C for 2 h in an argon atmosphere at a pressure of 2.5×10^4 Pa to ensure their homogenization.

Rods (16 mm diameter) of industrial steels were used in the as-received condition (without any additional heat treatment). The content of main components of a 13% Cr steel was 85.2% Fe, 13.6% Cr, 0.38% C, 0.30% Mn, 0.30% Si and 0.20% Ni. 25% Cr steel contained 72.8% Fe, 25.2% Cr, 0.13% C, 0.50% Mn, 0.46% Si, 0.45% Ni and 0.28% Ti.

The microstructure of Fe–Cr alloys consisted of the body centered cubic α-phase (ferrite), while that of the steels also contained fine inclusions of iron and chromium carbides.

Specimens in the form of tablets, 11.28 mm in diameter (1.0 cm^2 area) and 5.5 mm high, were machined from the Fe–Cr alloy and steel rods. Flat sides of the tablets were ground and polished mechanically.

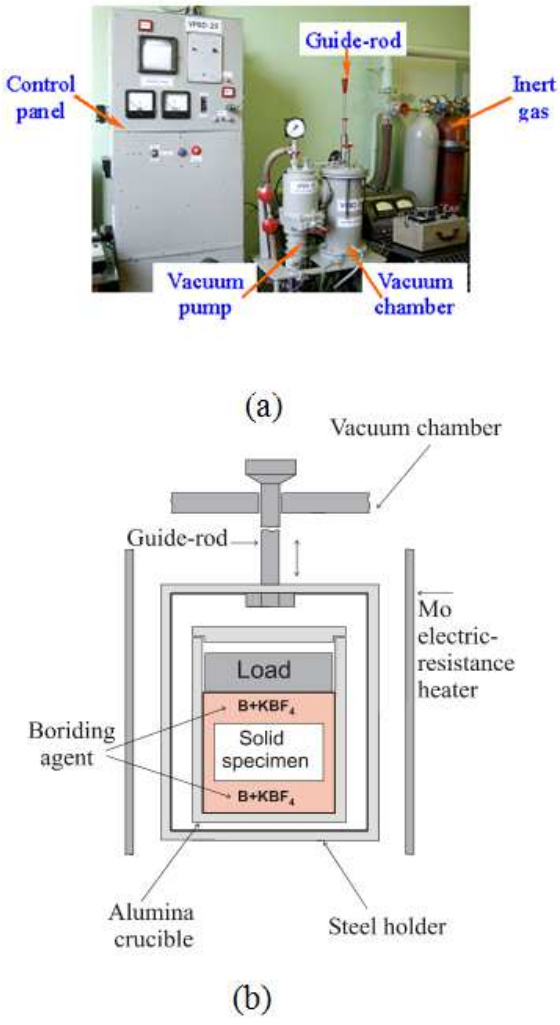

Fig. 1. Vacuum device employed for boriding Fe–Cr alloy and steel samples: (a) general view and (b) experimental cell.

2.2. Investigation Techniques

The vacuum device VPBD-2S employed for boriding Fe–Cr alloy and steel samples and its experimental cell are shown in

Fig. 1. Experiments were carried out in an alumina crucible, 13 mm inner diameter and 40 mm high. An alloy or steel tablet was embedded into a mixture of boron powder with 5% KBF_4 as an activator. This amount of KBF_4 is considered to be optimum [1, 29]. Experimental procedure was described in more detail elsewhere [28].

The temperature was maintained constant within ± 1°C with the help of an automatic thermoregulator VRT-3. Its measurements were carried out using a Pt-PtRh thermocouple. The experiments were carried out at a temperature of 850, 900 and 950°C. Their duration was 3600–43200 s (1–12 h).

After the experiment, the tablet with boride layers was cut along the cylindrical axis into two unequal parts (7 and 4 mm) using an electric-spark machine. Its greater part was embedded into a cold-setting epoxy resin and used to prepare a metallographic cross-section. The lesser part was used for X-ray diffraction investigations (plan-view samples).

Characterization of initial alloy and steel samples and boride layers formed was carried out with the help of metallography, X-ray diffraction (XRD) and chemical (CA) analyses, and electron probe microanalysis (EPMA). The thickness of boride layers was evaluated using the pictures obtained on an optical microscope MIM-7 equipped with a HP Photosmart 720 camera. Typically, six pictures were taken at different places of the interface (~ 1 cm long on any cross-section) between the reacting phases. The thickness of each boride layer was calculated by dividing the area occupied by that layer by the length of a region under examination, and the average value of six measurements was found.

Micrographs (backscattered electron images – BEI), contents of boron, iron and chromium in boride layers, and concentration profiles of these elements in the transition zone between reacting phases were obtained using an electron probe microanalyzer JEOL Superprobe 733. Accelerating voltage was 15 kV, while the current was 2×10^{-7} A. The beam spot diameter and the phase volume analyzed at each point were estimated to be about 1 μm and 2 μm^3, respectively.

Boron, iron and chromium standards (≥99.99% each) were employed. Measurements of element contents were treated using a versatile ZAF (atomic number, absorption and fluorescence corrections) program PACM. All three elements (B, Fe and Cr) were determined simultaneously, and the composition was then normalized to 100%. Non-normalized values usually fall in the range 98-102%, providing evidence for a rather good accuracy of measurements, especially in view of the huge difference (more than two orders of magnitude) in intensity of radiation from boron and that from iron or chromium.

X-ray diffraction (XRD) patterns were taken immediately from the surface of tablet plan-view samples on a DRON-3 apparatus equipped with both a computer and a self-recording potentiometer KSP-4. These were obtained at a step of 0.02°, detector rotational speed 0.0167° s^{-1} (1° min^{-1}) and sample rotational speed 62.83 rad s^{-1} (600 rpm). The counting time was 10 s at 400 imp s^{-1} and the velocity of the tape movement was 0.167 mm s^{-1} (600 mm h^{-1}). Use was made of Cu K_α radiation.

Before taking the first X-ray diffraction pattern, both flat surfaces of a borided tablet sample were slightly polished just to smoothen available elevations around 1 μm high. This practically as-received surface of the tablet was considered to be Section 0 of the sample. Then, 10 to 30 μm of a boride layer (depending upon its total thickness) was removed from the flat surface of the tablet by grinding and subsequent polishing, and another X-ray diffraction pattern was taken (Section I). This procedure was repeated at a step of 30-50 μm until the base material was reached. Five to eight X-ray diffraction patterns were thus taken on each borided alloy or steel sample.

Microhardness measurements on metallographic cross-sections were carried out using a standard PMT-3 tester with the diamond pyramid (Vickers indenter). The load was 0.98 N (100 g).

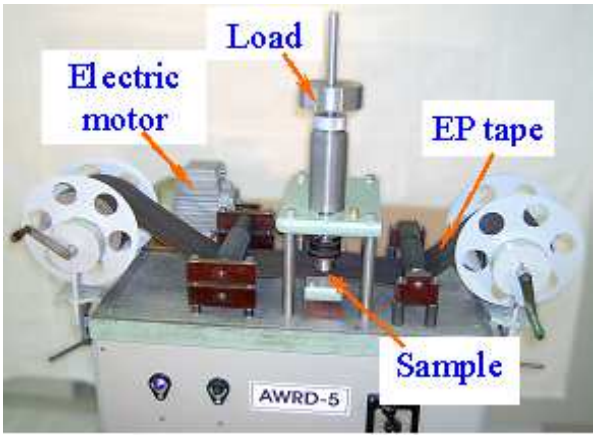

Fig. 2. AWRD-5 device for dry abrasive wear resistance tests of borided samples.

Dry abrasive wear resistance tests of borided alloy and steel samples were carried out in the sliding mode on P180 SiC emery paper (EP) tape (main fraction grain size 63 μm, maximum 90 μm) using an AWRD-5 device shown in Fig. 2. The velocity of continuous movement of the tape (25.0 m long, 0.12 m wide) was 0.35 m s^{-1}, while the gauge length during each test was 22.0 m. The load was 50 N (5.1 kg). Each test was carried out along a fresh track on the tape to ensure identical conditions for all samples. The wear resistance was determined by means of weighing a sample and measuring its height before and after the test.

3. Results and Discussion

3.1. Phase Identity and Chemical Composition of Boride Layers

With all the alloy and steel samples investigated, two continuous boride layers were generally found to form in a coating at the interface between the reactants at a temperature of 850, 900 and 950°C but not always their formation was simultaneous. The constituent phases of the layers were identified by plan-view layer-by-layer X-ray diffraction analysis as shown schematically in Fig. 3 for Fe–5% Cr and Fe–30% Cr alloys.

Comparison of our experimental X-ray patterns with the literature data for iron and chromium borides [30–35] indicated that in the case of 5–15% Cr alloys and 13% Cr steel the outer boride layer bordering the boriding agent consists of a solid solution based on the FeB chemical compound, whereas the inner boride layer adjacent to the solid substrate consists of a solid solution based on the Fe2B chemical compound as exemplified in Fig. 4 for a Fe–15% Cr alloy.

The strongest reflections were found to be {002} ($2\theta = 63.07^{o}$ and spacing, $d = 0.1474$ nm) and, to a lesser extent, {020} ($2\theta = 32.63^{o}$ and $d = 0.2744$ nm) for the orthorhombic FeB phase, and {002} ($2\theta = 42.55^{o}$ and $d = 0.2125$ nm) for the tetragonal Fe_2B phase. It should be noted that with isotropic microcrystalline samples the strongest reflections are {111}, {200} and {210} for FeB and {211} for Fe_2B [30–33].

It means that both layers possess a pronounced {002} texture and therefore consist of columnar crystals oriented preferentially in the direction of diffusion. This is considered to be a consequence of the existence of paths of enhanced diffusion in the crystal lattices of FeB and Fe_2B [1, 12]. If such paths are not available (close rates of diffusion in all crystallographic directions), almost flat boride layers are formed (see, for example, [29]).

The change in intensities of most characteristic reflections with increasing distance from the surface of a borided Fe–15% Cr alloy tablet is illustrated in Fig. 5 as an example. Numerical values of intensities presented in Table 1 provide evidence that the larger orientation order is observed for the inner portions of both boride layers compared to their near-interface portions. This is easily explainable because near-interface portions of any boride layer are less equilibrated compared to its inner portions. Therefore, near-interface crystals have less time to align in the preferred direction. More details about the process of ordering of any boride layer eventually resulting in the formation of its texture, as illustrated in Fig.6, can be found, for example, in the works [1, 12].

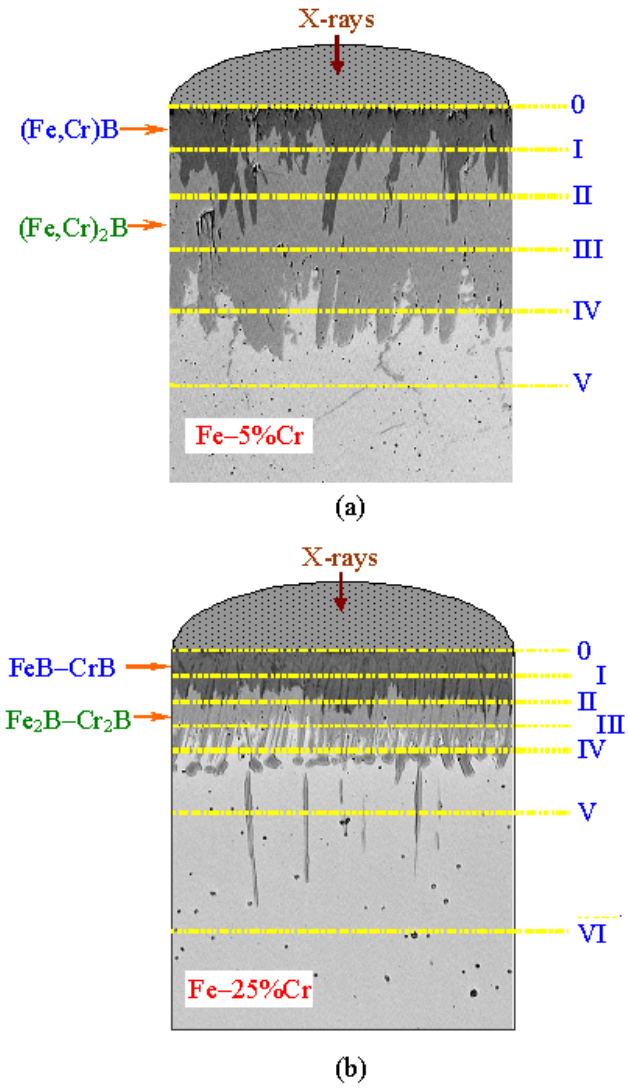

Fig. 3. Scheme of X-ray diffraction investigations of borided (a) Fe–5% Cr and (b) Fe–25% Cr alloy samples. Boriding conditions: 950°C, 21600 s (6 h).

X-ray investigations were followed by EPMA measurements to find out the chemical composition of an appropriate boride layer in its different sections from one interface to another. As seen in Fig. 3a, Section 0 of a borided Fe–5% Cr sample corresponded to the FeB phase. Average Fe, Cr and B contents of this and other phases, found by EPMA measurements on X-ray diffraction samples, are provided in Table 2. Sections I and II crossed both the FeB and Fe2B phases, with the amount of the FeB phase in Section I (Fig. 7a) being larger than that in Section II (Fig. 7b). Only the Fe2B phase was present in Section III (Fig. 7c). The microstructure of Sections IV consisted of Fe2B and the alloy base <Fe> insignificantly depleted in chromium compared to its content in the alloy, while that of section V was entirely the alloy base <Fe> of nominal composition 95% Fe–5% Cr.

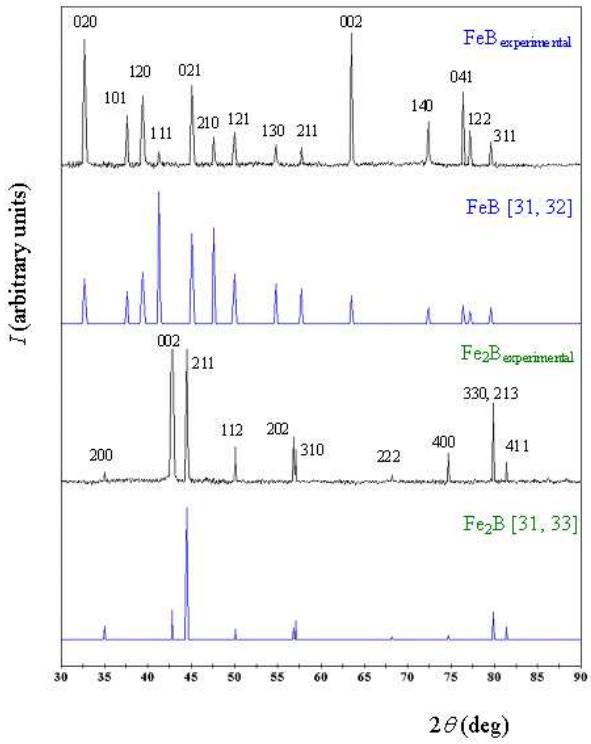

Fig. 4. Comparison of experimental and literature [31–33] X-ray diffraction patterns of the FeB and Fe_2B phases formed at the Fe–15% Cr alloy–boron interface after thermochemical boriding at 950°C for 21600 s (6 h). The experimental pattern of the FeB phase corresponds to Section 0, while that of Fe_2B phase approximately to Section III of Fig. 3a.

As seen in Table 2, the solubility of chromium in the FeB i Fe_2B phases formed during thermochemical boriding of Fe–5% Cr alloy samples is rather high. Actually, it does not differ considerably from its content in the alloy base. The average content of the components in the outer boride layer is 16.3% (50.0 at.%) boron, 79.5% (47.3 at.%) iron and 4.2% (2.7 at.%) chromium that corresponds to the stoichiometry of a solid solution based on the phase FeB.

Chemical composition of the inner boride layer is 8.9% (33.4 at.%) boron, 86.6% (63.1 at.%) iron and 4.5% (3.5 at.%) chromium. These values are in fair agreement with the stoichiometry of a solid solution based on the phase Fe_2B. The Fe_2B layer bordering immediately the alloy base contains somewhat more chromium than the more distant FeB layer.

The chromium content was found to be 6 ± 1 at.% in the (Fe,Cr)B layer and 7± 2 at.% in the $(Fe,Cr)_2B$ layer with a Fe–10% Cr alloy [19] and 8 ± 1 at.% in the (Fe,Cr)B layer and 12 ± 2 at.% in the $(Fe,Cr)_2B$ layer with a Fe–15% Cr alloy [24]. These values agree fairly well with findings of other authors [9, 36].

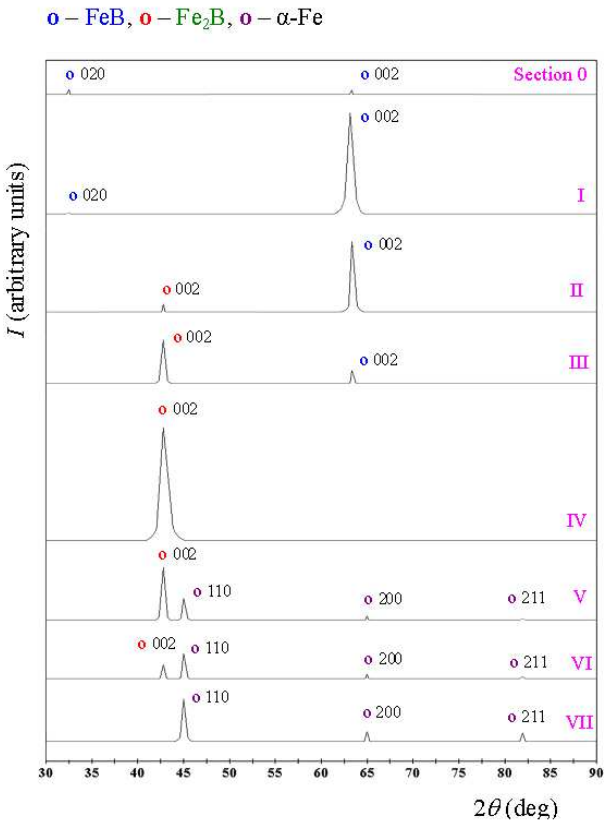

Fig. 5. Most intensive reflections of X-ray diffraction patterns taken from different plan-view sections of a Fe–15% Cr alloy sample borided at 950°C for 21600 s (6 h), see also Figs 3 and 4, and Table 1.

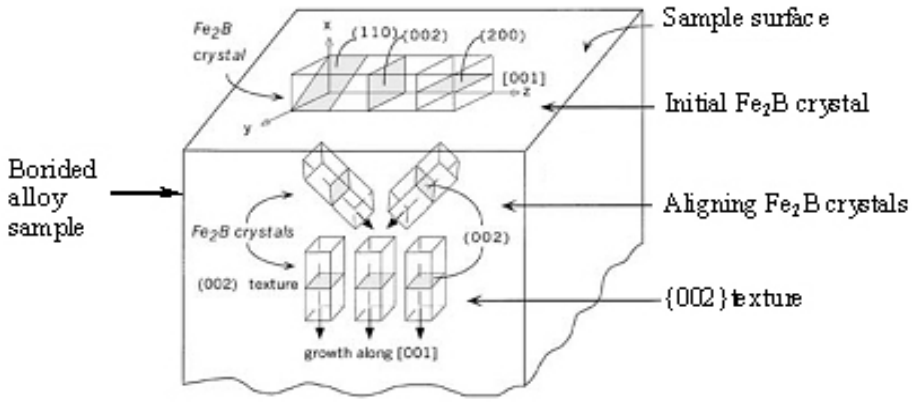

Fig. 6. Schematic illustration of aligning the Fe_2B crystal with the formation of texture of the Fe_2B layer [12]

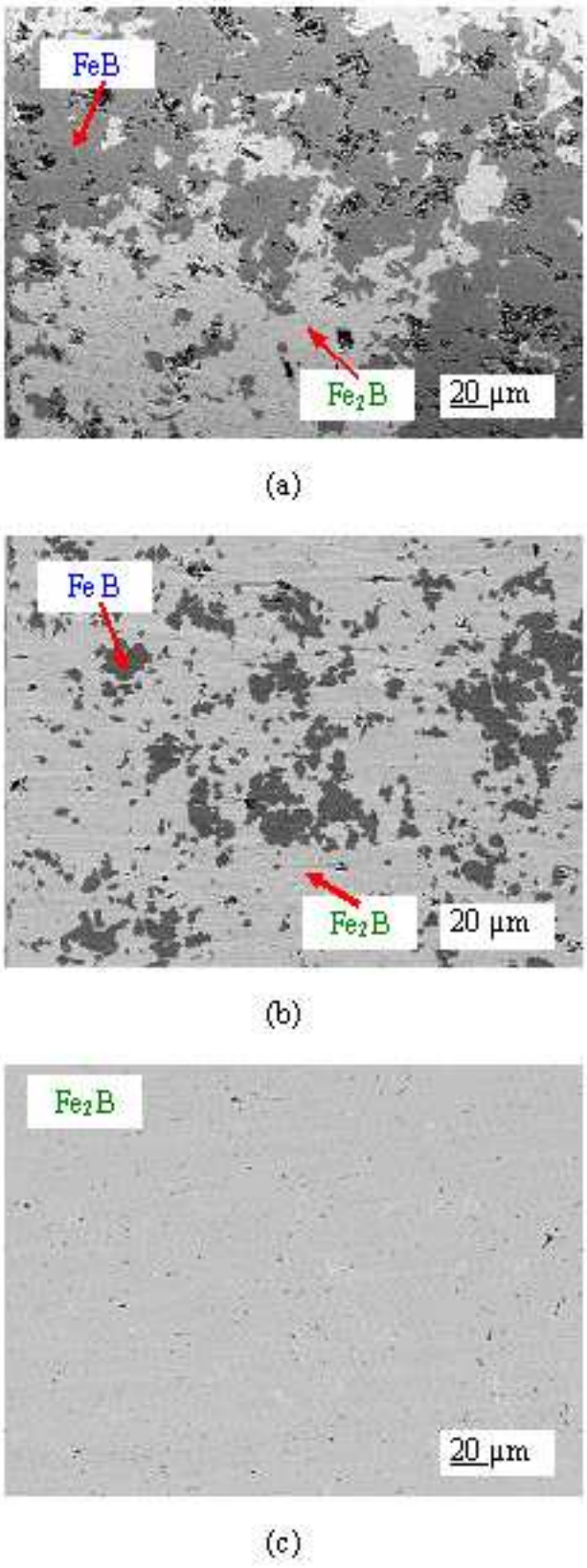

Fig. 7. Microstructure of a Fe–5% Cr alloy sample borided at 950°C for 21600 s (6 h) in Section (a) I, (b) II and (c) III, see also Fig. 3a.

Since both phases FeB and Fe_2B dissolve considerable amounts of chromium, their chemical formulae should be more exactly expressed as (Fe,Cr)B and $(Fe,Cr)_2B$, respectively. Simplified designations FeB and Fe_2B will only used for brevity.

As seen from Table 3, EPMA measurements across boride layers did not reveal any homogeneity ranges of the FeB and Fe_2B phases. The contents of the components Fe, Cr and B were the same within the error of determination (± 0.5%) at both interfaces of any boride layer, whereas in the case of existence of a noticeable homogeneity range they would gradually change from one interface to another.

The distribution of the components within the transition zone between the reacting phases is shown for a Fe–5% Cr alloy in Fig. 8 as an example. It is rather irregular (especially for boron) due, firstly, to non-equilibrium conditions of formation of the layers and, secondly, to their columnar morphology, so that the scan line crosses a few different crystals across the layer width. Nonetheless, judging from this figure the lack of homogeneity ranges of the FeB and Fe_2B phases can hardly be doubted.

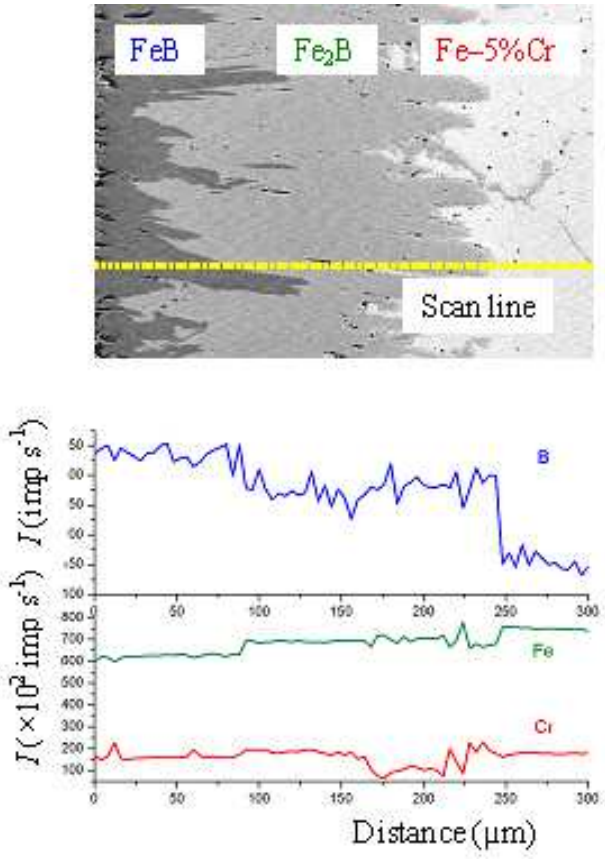

Fig. 8. Microstructure of the transition zone between a Fe–5% Cr alloy and boron, and concentration profiles of boron, iron and chromium. Boriding conditions: temperature 950°C, reaction time 21600 s (6 h).

Table 1. X-ray diffraction data showing preferential directions of growth for the FeB and Fe_2B phases formed at the interface of a Fe–15% Cr alloy and boron after boriding at a temperature of 950°C for 21600 s (6 h) – see also Fig. 5.

Phase	*HKL*	*d* (nm)	Peak intensity (arbitrary units)							
			0#	I	II	III	IV	V	VI	VII
FeB	020	0.275	150	17	9					
	002	0.148	128	2500	1750	332				
Fe_2B	002	0.212			215	1080	2800	1300	350	
	110	0.201						538	625	1050
α-Fe	200	0.143						103	120	250
	211	0.117						42	55	219

Serial numbers of appropriate sections of a borided tablet sample by a plane parallel to its flat surface (Section 0, I and so on, deeper into the sample bulk – see Fig. 3).

Table 2. Average Fe, Cr and B contents of reacting phases, found by EPMA measurements on borided Fe–5% Cr alloy samples after their X-ray diffraction investigations – see also Figs 3 and 7.

Section in Fig. 3a	Region	Content (mass%/at.%)			Phase
		Fe	Cr	B	
0	One-phase	79.5/47.3	4.2/2.7	16.3/50.0	(Fe,Cr)B
I	Darker in Figs 3a and 7a	80.0/48.1	4.1/2.6	15.9/49.3	(Fe,Cr)B
	Brighter in Figs 3a and 7a	86.1/62.3	4.8/3.8	9.1/33.9	$(Fe,Cr)_2B$
II	Darker in Figs 3a and 7b	79.0/46.5	4.3/2.7	16.7/50.8	(Fe,Cr)B
	Brighter in Figs 3a and 7b	87.0/63.7	4.4/3.4	8.7/32.8	$(Fe,Cr)_2B$
III	One-phase	86.6/63.1	4.5/3.5	8.9/33.4	$(Fe,Cr)_2B$
IV	Darker in Fig. 3a	87.1/63.7	4.2/3.3	8.7/33.0	$(Fe,Cr)_2B$
	Brighter in Fig. 3a	95.1/94.8	4.9/5.2	0.0/0.0	<Fe>
V	One-phase	95.0/94.6	5.0/5.4	0.0/0.0	<Fe>

Table 3. EPMA data for the Fe–10% Cr alloy–boron diffusion zone illustrating the lack of any noticeable homogeneity ranges of the FeB and Fe_2B phases. Boriding conditions: temperature 950°C, reaction time 21600 s (6 h).

Phase	Place of measurement	Content (at.%)			Remarks
		Fe	Cr	B	
At distance l away from the alloy-boride layer interface					
Fe–Cr	l = –100 μm	89.7	10.3	0.0	<Fe>
	–50	89.6	10.4	0.0	
	–30	89.4	10.6	0.0	
	–20	88.1	10.3	1.6	
	–10	89.5	10.5	0.0	
Inner boride layer	10	59.6	7.1	33.3	$(Fe,Cr)_2B$
	20	59.7	7.3	33.0	
	30	61.2	6.5	32.3	
	40	58.9	7.8	33.3	
	50	59.4	6.5	34.1	
	60	61.5	5.1	33.4	
	70	59.3	9.1	31.6	
	80	59.0	8.0	33.0	
	90	44.4	5.9	49.7	
Outer boride layer	100	43.1	5.1	51.7	(Fe,Cr)B
	110	44.5	6.3	49.2	
	120	44.7	6.0	49.3	
	130	43.3	5.3	51.4	
	140	44.0	6.3	49.8	
	150	43.2	5.0	51.7	

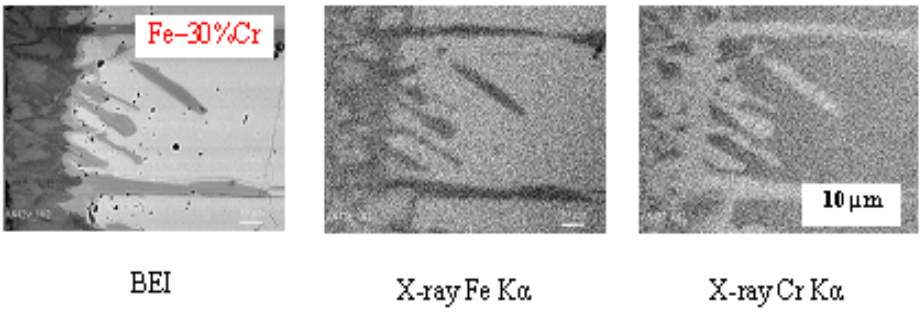

Fig. 9. Cross-sectional backscattered electron image (BEI) of the transition zone between a Fe–30% Cr alloy and boron, and X-ray maps for iron and chromium. The brighter the region, the higher is the content of an appropriate element (Fe or Cr). Boriding conditions: 950°C, 21600 s (6 h).

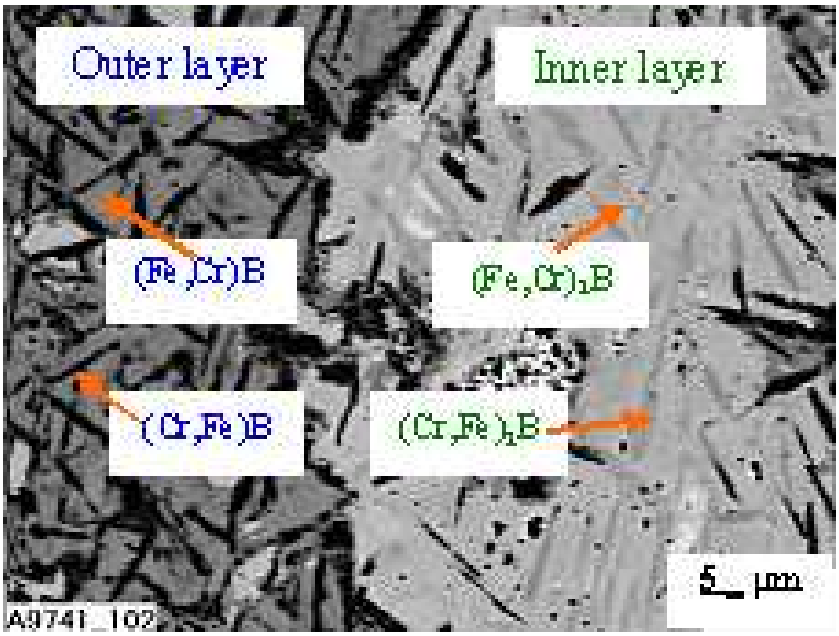

Fig. 10. Plan-view micrograph (BEI) corresponding to the second section for a Fe–30% Cr alloy sample borided at 850°C for 43200 s (12 h). The dark area is the outer boride layer. Its brighter regions are the (Fe,Cr)B phase, while the darker regions are the (Cr,Fe)B phase. The bright area is the inner boride layer. Its brighter regions are the $(Fe,Cr)_2B$ phase, while the darker regions are the $(Cr,Fe)_2B$ phase.

Somewhat unexpectedly, X-ray diffraction analysis has only indicated the presence of FeB and Fe_2B and the entire absence of reflections of any chromium boride, even on the surface of borided samples of Fe–25% Cr and Fe–30% Cr alloys and a 25% Cr steel. Their X-ray diffraction patterns were similar to those for borided samples of Fe–5% Cr, Fe–10% Cr and Fe–15% Cr alloys and a 13% Cr steel (see Fig. 4).

In view of the relatively high chromium content (25% or more) in Fe–25% Cr and Fe–30% Cr alloys and a 25% Cr steel, of seven known compounds CrB_4, CrB_2, Cr_2B_3, Cr_3B_4, CrB, Cr_5B_3 and Cr_2B [36], the formation of at least CrB and Cr_2B phases could be expected. Besides, in this case the microstructure of both boride layers is readily seen visually in Figs 3b, 9 and especially 10 to be two-phase.

Table 4. Average Fe, Cr and B contents of boride phases, found by EPMA measurements on a borided Fe–30% Cr alloy samples used for X-ray diffraction investigations (see Figs 3b and 10).

Region in Fig. 10	Content (mass %/at.%)			Phase
	Fe	Cr	B	
Brighter of the outer boride layer	65.4/38.4	18.0/11.4	16.5/50.2	(Fe,Cr)B
Darker of the outer boride layer	39.8/23.5	44.3/28.1	15.9/48.4	(Cr,Fe)B
Brighter of the inner boride layer	76.9/55.7	14.2/11.1	8.9/33.2	(Fe,Cr)2B
Darker of the inner boride layer	28.1/19.7	62.8/47.3	9.1/33.0	(Cr,Fe)2B

With each layer, it consists of distinct brighter and darker regions. EPMA measurements presented in Table 4 for a Fe–30% Cr alloy clearly indicate that iron prevails in brighter regions, while chromium is dominant in darker ones. Similar results were also obtained for a Fe–25% Cr alloy and a 25% Cr steel.

Thus, the outer boride layer consists of a mixture of crystals of the (Fe,Cr)B and (Cr,Fe)B phases, having a peculiar regular arrangement. Nonetheless, even most strong reflections of CrB (spacing, d = 0.2350, 0.1965 and 0.1255 nm) and Cr_2B (d = 0.2590, 0.2158 and 0.2043 nm) [30, 31, 35] were missing from our experimental X-ray patterns.

Most probably, presence of the CrB phase in boride layers can hardly be revealed by XRD or any other method of structural analysis such as electron diffraction because under highly non-equilibrium conditions the lattice rearrangement FeB → CrB is not completed in view of time limitations. Therefore, part of iron sites of the FeB lattice, very similar to that of CrB, is merely replaced by chromium atoms, without any noticeable structural changes.

In other words, the non-equilibrium CrB phase crystallizes in the FeB lattice. Hence, being far from equilibrium, the outher boride layer appears to be single-phase structurally (crystallographically) and two-phase compositionally (chemically).

Similar considerations are also applicable to another pair Fe_2B and Cr_2B that are the constituents of the inner boride layer. Therefore, formation of the (Cr,Fe)B and $(Cr,Fe)_2B$ phases, readily seen visually in the microstructure of boride layers occurred on the surface of borided samples of Fe–25% Cr and Fe–30% Cr alloys and a 25% Cr steel, can hardly be doubted.

With materials of complicated chemical composition such as high-alloy steels, the two-phase microstructure of boride layers is much less profound in view of the strong influence of other elements (C, P, S, Si, Mn, *etc*.). Perhaps, just for this reason it was overlooked by previous researchers.

Thus, comparative analysis of the microstructure of all the alloys and steels investigated provides evidence for the existence of its two types as illustrated in Fig. 11. The first type (Type I) is exhibited by Fe–5% Cr, Fe–10% Cr and Fe–15% Cr alloys and a 13% Cr steel In this microstructure, each of two boride layers formed consists of a homogeneous phase either (Fe,Cr)B or $(Fe,Cr)_2B$ (Fig. 11b and d).

The second (Type II) is characteristic of Fe–25% Cr and Fe–30% Cr alloys and a 25% Cr steel. In this type of microstructure, each of two boride layers is two-phase, with the outer layer consisting of the (Fe,Cr)B and (Cr,Fe)B phases (Fig. 11b' and d') and the inner consisting of the $(Fe,Cr)_2B$ and $(Cr,Fe)_2B$ phases. As seen in Fig. 11b', the microstructure of the second type has a distinguishable network-platelet arrangement that is much less profound for a 25% Cr steel (Fig. 11d') than for Fe–25% Cr and Fe–30% Cr alloys.

3.2. Sequence and Mechanism of Formation of Boride Layers

Figure 12 provides evidence that the FeB and Fe_2B layers occur sequentially, with the Fe_2B layer being the first to form and grow. In the case of a Fe–5% Cr alloy, a continuous FeB layer is formed when the thickness of the Fe_2B layer exceeds, depending on the temperature of reaction, 100–180 μm.

After a 3600 s (1 h) reaction time at 950°C, the FeB layer is seen in Fig. 13 to be still missing from the Fe–10% Cr alloy–boron interface, even though the Fe_2B layer has already reached a thickness of around 70 μm. 7200 s (2 h) reaction time results in the formation of the FeB and Fe_2B layers at this temperature. 3600 s (1 h) reaction time in the temperature range of 850–950°C was found to be sufficient for both boride layers to form on the surface of samples of other alloys and steels investigated. An example with a Fe–25% Cr alloy is provided in Fig. 14.

Mechanism of formation of boride layers in a coating on the surface of alloy or steel samples appears to be as follows (for more detail, see [28, 37-40]. Initially, reacting phases are in immediate contact with each other. Therefore, the Fe_2B layer can readily grow at the Fe–B interface by direct chemical reaction between the surface iron and boron atoms

$$2Fe_{surf} + B_{surf} = Fe_2B \quad (1)$$

as shown schematically in Fig. 15.

To simplify the designations and further analytical treatment of kinetic data, iron and chromium will be considered as a single chemical element (Fe). In view of the close similarity of their physico-chemical properties, this simplification does not appear to cause any misleading results.

It must be clear, however, that the formation of the Fe_2B layer, even a few crystal-lattice units thick, separates the reactants from one another. Hence, further progress of the direct chemical reaction between the surface iron and boron atoms proves to be impossible.

Subsequently, the Fe_2B layer grows at the expense of counter-diffusion of iron and boron atoms across its bulk that is followed by two partial chemical reactions

$$2Fe_{dif} + B_{surf} = Fe_2B \quad (2_1)$$

and

$$B_{dif} + 2Fe_{surf} = Fe_2B \quad (2_2)$$

proceeding at the B–Fe_2B and Fe_2B–Fe interfaces, respectively, as shown in Fig. 16.

Note that no reaction can take place between the diffusing iron and boron atoms in the bulk of the growing Fe_2B layer. Any chemical transformations (reactions) proceed entirely at the layer interfaces.

After the continuous layers of both iron borides have formed (Fig. 17), their subsequent growth under conditions of reaction (chemical) control, when the rate of diffusion of reacting atoms across their bulks exceeds the rate of interfacial transformations, is generally due to four partial chemical reactions

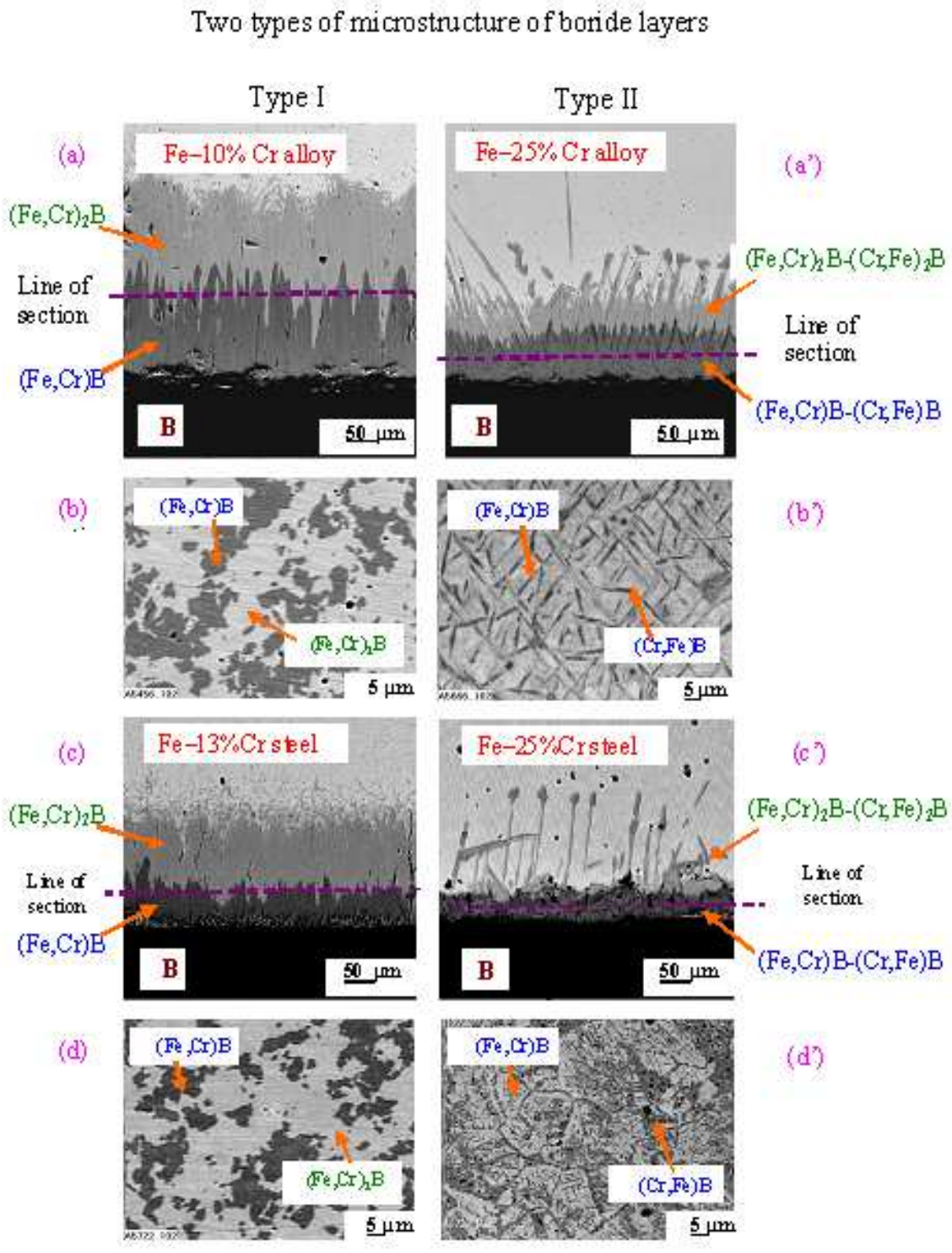

Fig. 11. Backscattered electron images (BEI) of the transition zone between reacting phases illustrating two types of microstructure of boride layers, and those of their plan-view sections shown by a line of section. Boriding conditions: 950°C, 21600 s (6 h).

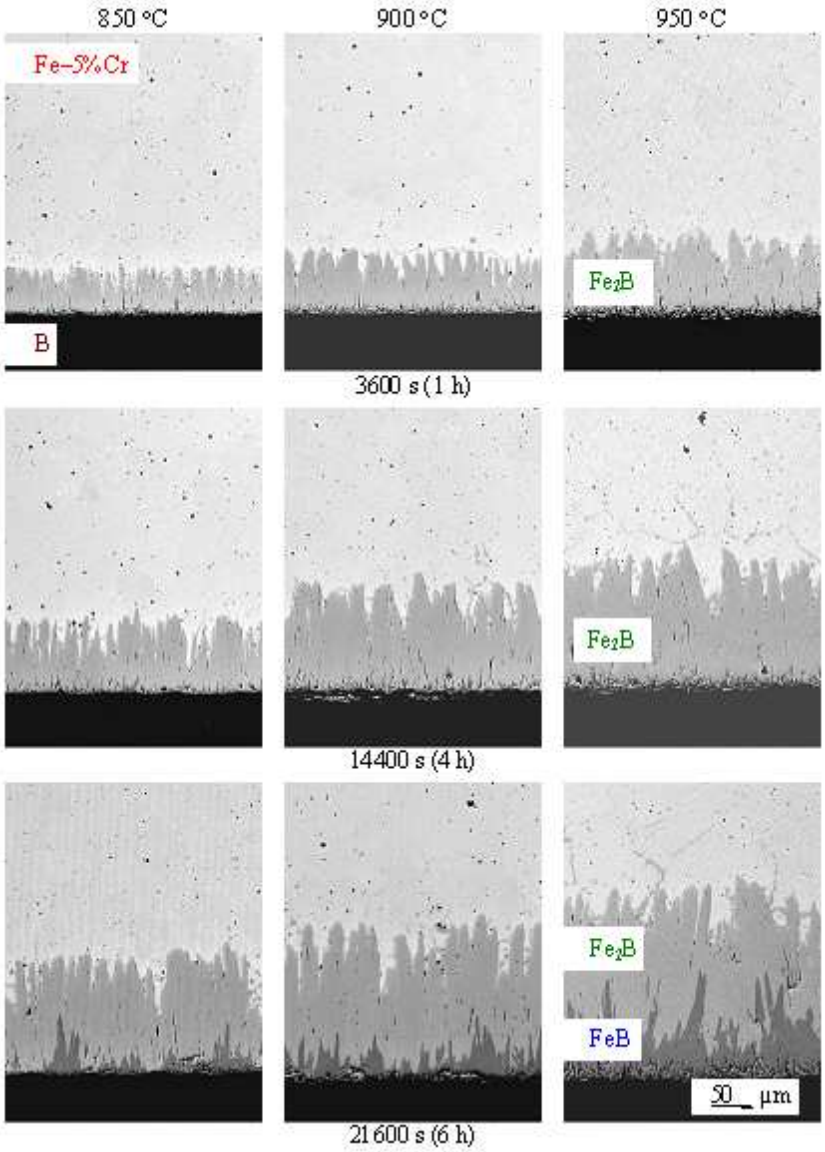

Fig. 12. Backscattered electron images (BEI) of the transition zone between a Fe–5% Cr alloy and boron. The Fe_2B layer is the first to occur and grow in a time range of 3600–14400 s (1–4 h). The next FeB layer is only formed when the thickness of the first becomes more than 100–180 µm.

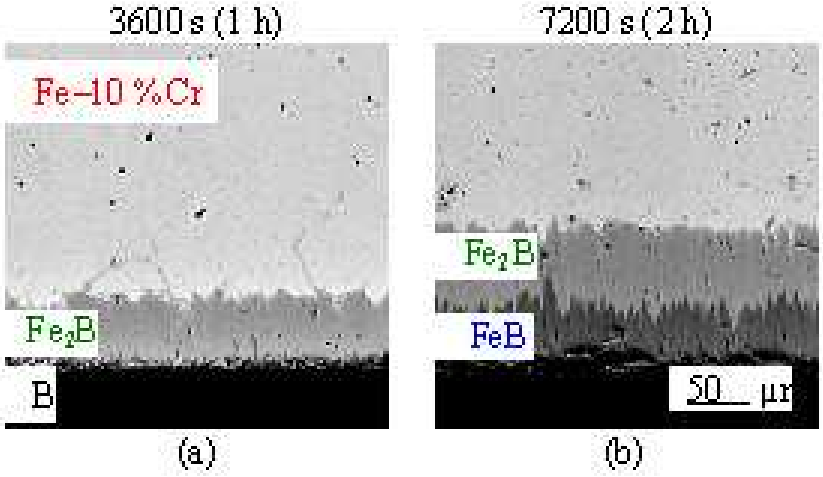

Fig. 13. Backscattered electron images (BEI) of the Fe–10 % Cr alloy–boron transition zone at 950°C. The Fe_2B layer is the first to occur.

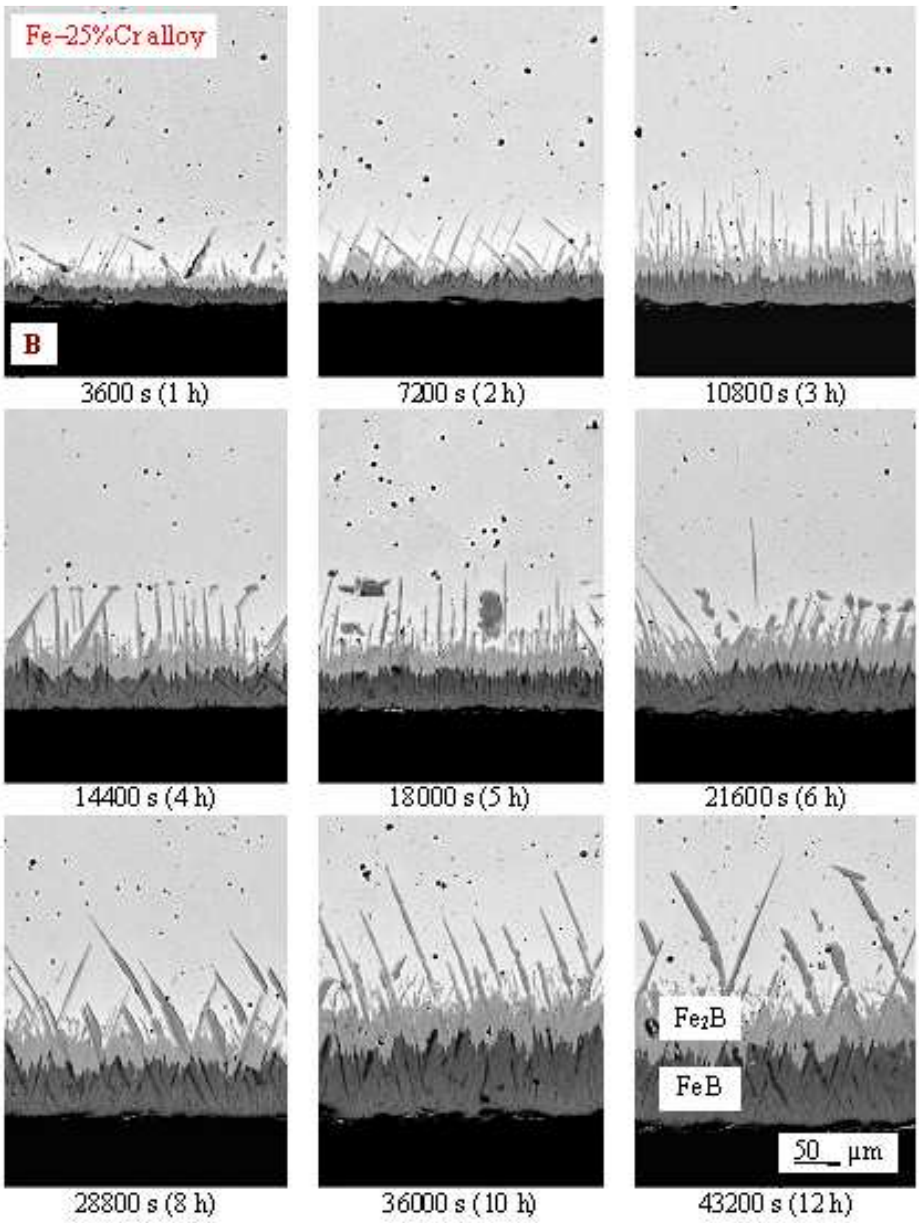

Fig. 14. Backscattered electron images (BEI) of boride layers formed at the Fe–25 % Cr alloy–boron interface at a temperature of 950°C. The darker layer bordering the boriding agent B is the FeB phase, while the brighter layer adjacent to the Fe–Cr alloy base is the Fe_2B phase.

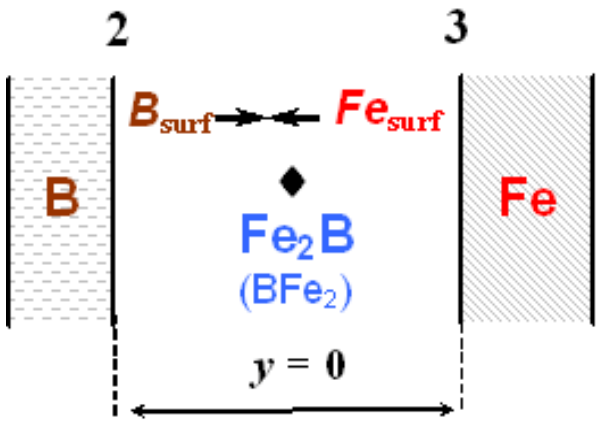

Fig. 15. Schematic diagram to illustrate the growth process of the Fe_2B layer by direct chemical reaction between the surface iron and boron atoms.

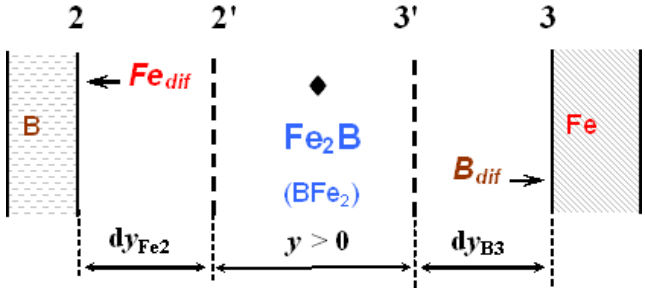

Fig. 16. Schematic diagram illustrating the growth process of the Fe_2B layer by partial chemical reactions between the diffusing iron atoms and surface boron atoms at interface 2 and between the diffusing boron atoms and surface iron atoms at interface 3.

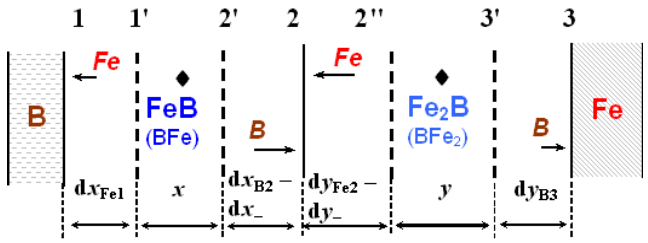

Fig. 17. Schematic diagram illustrating the growth process of the FeB and Fe2B layers under conditions of reaction (chemical) control. Arrows of different length are employed to indicate the decrease in amount of diffusing atoms, available at a particular interface, with increasing distance from an appropriate initial substance (B or Fe).

Layer	Interface	Reaction	
FeB	1	$Fe_{dif} + B_{surf} = FeB,$	(3_1)
	2	$B_{dif} + Fe_2B = 2FeB,$	(3_2)
Fe_2B	2	$Fe_{dif} + FeB = Fe_2B,$	(4_1)
	3	$B_{dif} + Fe_{surf} = Fe_2B.$	(4_2)

Obviously, thickening of the FeB and Fe_2B layers with passing time eventually results in a change of the regime of their growth from reaction controlled to diffusion controlled, when the rate of interfacial transformations (reactions) becomes first equal to, at certain critical layer thickness, and then greater than, at layer thicknesses exceeding this critical value, the rate of diffusion of appropriate reacting atoms to the reaction sites (interfaces) (for more detail, see [37-40]). After the FeB layer has reached its critical thickness with regard to boron, the Fe_2B layer loses the source of boron atoms and therefore stops growing at the expense of diffusion of this component. Note that the only source of boron atoms for both layers to grow is the initial boron phase (boron powder).

Again, after the Fe_2B layer has reached its critical thickness with regard to iron, the FeB layer loses the source of iron atoms and therefore stops growing at the expense of diffusion of this component. It must be clear that the only source of iron atoms for both layers to grow is the initial iron-containing phase (Fe–Cr alloy or steel).

Hence, under conditions of diffusion control the FeB and Fe_2B layers are able to grow only at their common interface 2, as shown in Fig. 18. The FeB layer grows at the expense of diffusion of boron atoms across its bulk and their subsequent reaction (3_2) with the Fe_2B compound. The Fe_2B layer grows at the expense of diffusion of iron atoms across its bulk and their subsequent reaction (4_1) with the FeB compound. Chemical reactions (3_1) and (4_2) cannot take place because of the lack of appropriate diffusing atoms.

Even though both FeB and Fe_2B layers are often considered to grow entirely at the expense of diffusion of the single component boron across their bulks, it is impossible with compact layers having no macroscopic defects and therefore growing by the volume-diffusion mechanism. During diffusional growth, by definition, diffusion across the layer bulks is the rate-determining step, the interfacial partial chemical reactions being very fast. It means that all the boron atoms reaching interface 2 react with Fe_2B to form FeB at that interface. Since under conditions of diffusion control the ability of interface 2 to combine those atoms exceeds their diffusional transport across the FeB layer (slow diffusion followed by fast reaction), none of them can diffuse further to interface 3 and react with Fe to form Fe_2B according to reaction (4_2). This reaction can only take place either under conditions of reaction control when the flux of boron atoms from the initial B-containing phase is sufficient for both boride layers to grow or if the FeB layer is non-protective, due to the presence of cracks, fissures and other macroscopic defects, while boriding is carried out from a vapour or liquid phase.

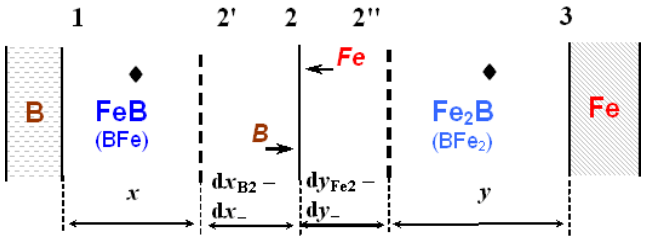

Fig. 18. Schematic diagram illustrating the growth process of the FeB and Fe2B layers under conditions of diffusion control. Both layers only thicken at their common interface 2. No partial chemical reactions can take place at interfaces 1 and 3 due to the lack of appropriate diffusing atoms (Fe at interface 1 and B at interface 3).

If boride layers are permeable to a vapour or liquid phase, direct chemical reactions between initial substances prove to be possible. Grain-boundary diffusion can also make a considerable contribution to the layer-growth process. If a few growth mechanisms are operative simultaneously, a complicated and hardly tractable microstructure of boride layers can readily be formed.

3.3. Layer-Growth Kinetics

Growth kinetics of compound layers, boride ones in particular, are conventionally treated from a diffusional viewpoint giving parabolic equations of the type $x^2 = 2k_1t$, where x is the layer thickness, k_1 is the layer growth-rate constant and t is the time [1, 37–39]. Such equations produce a quite satisfactory fit to the experimental data, as exemplified with rather thick FeB and Fe_2B boride layers investigated in Tables 5 and 6 where the initial experimental data (Table 5) and the average values of the layer growth-rate constant (Table 6) are presented for a Fe–5% Cr alloy.

Table 5. Thickness and kinetic constants for the FeB and Fe_2B layers formed at the Fe–5% Cr alloy-boron interface.

Temperature (°C)	Time ($\times 10^2$ s)	Thickness ($\times 10^{-6}$ m)			k_1 ($\times 10^{-13}$ m^2 s^{-1}) from the equation $x^2 = 2k_1t$		
		total	FeB	Fe_2B	total	FeB	Fe_2B
850	36	50	-	50	3.5	-	3.5
	72	74	-	74	3.8	-	3.8
	144	100	-	100	3.5	-	3.5
	216	156	30	126	0.563	0.0208	0.368
	288	187	40	147	0.607	0.0278	0.375
900	36	71	-	71	7.0	-	7.0
	72	100	-	100	7.2	-	7.2
	144	140	-	140	6.8	-	6.8
	216	205	45	160	0.973	0.047	0.593
	288	227	54	173	0.894	0.050	0.520
950	36	91	-	91	11.5	-	11.5
	72	130	-	130	11.7	-	11.7
	144	184	-	184	11.8	-	11.8
	216	227	60	167	1.193	0.083	0.646
	288	254	74	180	1.120	0.095	0.563

Table 6. Average values of the growth-rate constants for the FeB and Fe_2B layers formed at the Fe–5% Cr alloy-boron interface.

Temperature (°C)	Time range ($\times 10^2$ s)	k_1 ($\times 10^{-13}$ m^2 s^{-1})		
		total	FeB	Fe_2B
850	36–144	3.6	-	3.6
	216–288	0.585	0.0243	0.372
900	36–144	7.0	-	7.0
	216–288	0.934	0.049	0.557
950	36–144	11.7	-	11.7
	216–288	1.157	0.089	0.605

As evidenced from Fig. 19, the temperature dependence of the growth-rate constant of the Fe_2B layer in the time range 3600–14400 s (1–4 h) when the FeB layer is still missing between boron and the Fe_2B layer is described by a relation of the Arrhenius type. The least-squares fit method yields the following equation

$$k_1^{(Fe_2B)} = 7.00\times10–6 \exp(–135.0 \text{ kJ mol–1/RT}) \text{ m2 s–1}$$

where R is the gas constant (8.314 J mol –1 K –1) and T is the absolute temperature, K.

(1). It should be emphasized, however, that purely diffusional considerations and parabolic equations are generally insufficient to understand and explain a variety of known experimental observations. The main amongst those are as follows.

(2). Initial layer growth is known to be linear and not parabolic.

(3). In multiphase binary systems, formation of compound layers is more often sequential than simultaneous, whereas from a diffusional viewpoint they all must occur and then grow parabolically with passing time.

(4). Existence of a rather wide range of homogeneity is a necessary condition in derivation of parabolic equations but many, if not a majority of, chemical compounds have no homogeneity range. Nonetheless, their layers grow at a rate, sometimes even far exceeding that of the layers of compounds with a wide homogeneity range.

(5). According to diffusional considerations, any once formed compound layer of a multiphase binary system, cannot subsequently disappear, whereas experiments provide evidence that in artificially prepared reaction couples some of them can either grow or shrink, or even disappear entirely, depending on the ratio of their initial thickness.

These and other inconsistencies of a diffusional approach to layer-growth kinetics are readily overcome in the framework of a physico-chemical one (for more detail, see [37-40]). Unlike the former, the latter takes account both of the rate of diffusion across the bulks of growing compound layers and the rate of further chemical transformations at the layer interfaces.

Growth kinetics of the FeB and Fe_2B layers at the interface of a Fe–Cr alloy or steel and boron at the expense of diffusion of both components can generally be described by a system of two non-linear differential equations

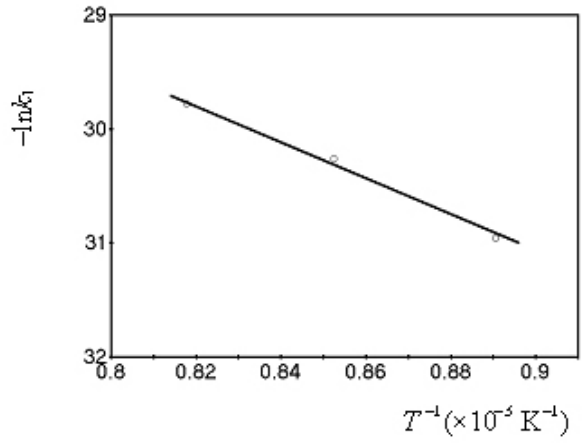

Fig. 19. Temperature dependence of the growth-rate constant of the Fe2B layer in the time range 3600–14400 s (1–4 h) in the absence of the FeB layer.

$$\frac{dx}{dt} = \frac{k_{0Fe1}}{1+\frac{k_{0Fe1}x}{k_{1Fe1}}} + \frac{k_{0B2}}{1+\frac{k_{0B2}x}{k_{1B2}}} - \frac{rg}{p}\,\frac{k_{0Fe2}}{1+\frac{k_{0Fe2}y}{k_{1Fe2}}} \qquad (5_1)$$

$$\frac{dy}{dt} = \frac{k_{0Fe2}}{1+\frac{k_{0Fe2}y}{k_{1Fe2}}} + \frac{k_{0B3}}{1+\frac{k_{0B3}y}{k_{1B3}}} - \frac{q}{sg}\,\frac{k_{0B2}}{1+\frac{k_{0B2}x}{k_{1B2}}} \qquad (5_2)$$

where x is the outer FeB layer thickness; y is the inner Fe_2B layer thickness; k_{0Fe1} and k_{0B2} are the chemical growth-rate constants of the FeB layer at the expense of diffusion of iron and boron atoms, respectively; k_{1Fe1} and k_{1B2} are the diffusional (physical) growth-rate constants of the FeB layer at the expense of diffusion of iron and boron atoms, respectively; k_{0Fe2} and k_{0B3} the chemical growth-rate constants of the Fe_2B layer at the expense of diffusion of iron and boron atoms, respectively; k_{1Fe2} and k_{1B3} are the diffusional (physical) growth-rate constants of the Fe_2B layer at the expense of diffusion of iron and boron atoms, respectively; g is the ratio of the molar volumes of the FeB and Fe_2B compounds; $p = q = r = 1$ and $s = 2$ (factors from the chemical formulae of FeB (written as BFe) and Fe_2B (BFe_2).

The value of g is determined from the density of the compounds FeB (BFe) $\rho_1 = 6.70 \times 10^3$ kg m^{-3} and Fe_2B (BFe_2) $\rho_2 = 7.34 \times 10^3$ kg m^{-3} [1] and their molecular mass $M_1 = 66.65$ g mol^{-1} and $M_2 = 122.49$ g mol^{-1}: $g = M_1\rho_2/M_2\rho_1 = 0.60$.

Initially, growth kinetics of compound layers is seen from a system of equations (5) to be linear because at low t the terms of the type k_0x/k_1 and k_0y/k_1 can be neglected in comparison with unity and therefore this system is simplified to

$$\frac{dx}{dt} = k_{0Fe1} + k_{0B2} - \frac{rg}{p}\,k_{0Fe2} \qquad (6_1)$$

$$\frac{dy}{dt} = k_{0Fe2} + k_{0B3} - \frac{q}{sg}\,k_{0B2} \qquad (6_2)$$

System of equations (6) describes the reaction controlled stage of growth of boride layers when the rates of diffusion of iron and boron atoms across layer bulks are so high that their effect on the overall rates of formation of the layers is negligible in comparison with that of the rates of subsequent chemical transformations taking place at phase interfaces. This is that case in which the purely chemical processes are rate-determining (chemical control), for there is a great excess of diffusing atoms of both kinds for both layers to grow.

It does not mean, however, that under such circumstances the FeB and Fe_2B layers will necessarily occur and grow at the alloy (steel)–boron interface simultaneously. Clearly, their simultaneous occurrence is only possible, if the derivatives dx/dt and dy/dt in equations (5) and (6) are positive, $dx/dt > 0$ and $dy/dt > 0$, and consequently the inequalities $k_{0Fe1} + k_{0B2} > (rg/p)k_{0Fe2}$ and $k_{0Fe2} + k_{0B3} > (q/sg)k_{0B2}$ are satisfied. In such a case, both boride layers will grow simultaneously from the very start of interaction of initial substances according to a linear law

$$x = (k_{0Fe1} + k_{0B2} - \frac{rg}{p}\,k_{0Fe2})t \qquad (7_1)$$

$$y = (k_{0Fe2} + k_{0B3} - \frac{q}{sg}\,k_{0B2})t \qquad (7_2)$$

Note that they grow at the highest rates possible under given (constant) temperature-pressure conditions. Linear stage of growth of boride layers has not yet been explored due probably to the necessity to carry out thorough experiments with very thin films.

If the condition

$$k_{0Fe1} + k_{0B2} < \frac{rg}{p}\,k_{0Fe2} \qquad (8)$$

is satisfied, the FeB layer cannot form at all ($dx/dt < 0$). Therefore, only the Fe_2B layer is observed to grow at the alloy (steel)–boron interface. If the FeB layer were in an artificially prepared sample, its thickness would decrease, and it might eventually disappear completely. In this case, the FeB layer is kinetically (not thermodynamically) unstable since the decrease in its thickness due to the consumption during growth of the Fe_2B layer by reaction (4_1) exceeds the increase due to reactions (3_1) and (3_2).

From the system (5), it is easy to see that the sequential formation of boride layers ($dx/dt < 0$, $dy/dt > 0$ or $dx/dt > 0$, $dy/dt < 0$) is more probable than simultaneous ($dx/dt > 0$ and $dy/dt > 0$), the ratio of probability being 2: 1. Besides, this system indicates a necessary condition for the occurrence of the next layer, if their formation is not simultaneous. Since the Fe_2B layer is the first to occur, the FeB layer can only start to form when $dx/dt > 0$ and hence

$$k_{0\mathrm{Fe1}} + k_{0\mathrm{B2}} \geq \frac{rg}{p} \frac{k_{0\mathrm{Fe2}}}{1 + \dfrac{k_{0\mathrm{Fe2}} y_{\min}}{k_{1\mathrm{Fe2}}}} \tag{9}$$

Where $y_{\min}$ is a smallest (*minimal*) thickness of the Fe_2B layer necessary for the FeB layer to occur and grow. Chemically, it merely means that at this thickness of the Fe_2B layer, the rate of consumption of the FeB layer during growth of the Fe_2B layer by reaction (4_1) becomes first equal to and then less than the rate of its growth due to reactions (3_1) and (3_2).

Note that the existing kinetic models of diffusional growth of boride layers (see, for example, [43–46]) are explicitly or tacitly based on an assumption of the existence of a rather wide range of homogeneity, *HR*, of appropriate borides, iron borides in particular. However, as follows from the available data on the phase equilibria in the binary system Fe–B [6–8] and the ternary system Fe–Cr–B [36], iron borides FeB and Fe_2B have no noticeable homogeneity range. Our experiments with Fe–Cr alloys and steels provide an additional proof of validity of these observations.

Also, the concentration profiles of the elements within the growing layers are assumed to be close to linear (see Fig. 1 in [44]). In such a case, the parabolic layer growth-rate constant, k_1, proves to be proportional to the diffusion coefficient, D, of a given component and the difference, Δc, in its concentration (content) at the interfaces of a growing compound layer: $k_1 \sim D\,\Delta c$. The latter is conventionally considered to be equal to the width of the homogeneity range, *HR*, of an appropriate compound: $\Delta c = HR$. If it were so, however, then the layers of compounds without any range of homogeneity would not grow at all, that contradicts available experimental data.

Again, for compounds with a narrow range of homogeneity these models yield the unrealistically high values of the diffusion coefficients because in the limit it means dividing by zero and hence $D \to \infty$, as $\Delta c \to 0$. From a physical viewpoint, such values are hardly possible.

In fact, the layer of any compound always grows at the expense of stoichiometry of that compound and not at the expense of its range of homogeneity. The value of Δc is the difference in concentration of vacancies at layer interfaces [37-40]). It is necessary to distinguish, however, between the newly-formed and native (equilibrium) vacancies. The newly-formed vacancies arise in the course of partial chemical reactions proceeding at layer interfaces. These are thus reaction-induced vacancies which do not exist in a given equilibrated compound. The native (inherent), mainly thermal, vacancies are present in the compound initially (in the equilibrium state), their amount being quite negligible by comparison, except perhaps at temperatures close to its melting point.

The concentration of newly-formed vacancies of a given component in a growing compound layer at its interface where a product-forming partial chemical reaction takes place is regarded to be numerically equal (with the opposite sign) to the content of this component in the compound, while that at another (non-reacting) interface zero (ideal case in which no native vacancies are available in the compound). Then $k_1 = D$, if $\Delta c = HR = 0$. Hence, the parabolic growth-rate constant, k_1, is identified with the diffusion coefficient, D, of a given component in the lattice of a chemical compound. If $HR \neq 0$, $k_1 \approx D$, with the difference between k_1 and D decreasing as *HR* tends to zero. In other words, the closer the compound to its stoichiometric composition, the more nearly k_1 approaches D. Thus, the two assumptions made allow a self-consistent approach, excluding dividing by zero and yielding physically reasonable values of the diffusion coefficient, D, to be developed.

It must also be emphasized that, contrary to wide-spread and nonetheless misleading views (examples are too numerous to cite here, appropriate references can readily be found in [37-40]), the role of native point defects, such as vacancies of a given component, in the reaction-diffusion process of formation of any chemical compound, like boriding, carburizing, metallization and others, is opposite to their role in the process of self-diffusion of that component in the compound taken as a separate phase.

In the absence of complicating factors, the *higher* the amount of native vacancies, the *higher* is the rate of self-diffusion of the component in the separate phase. Contrary to this, the *higher* the amount of native vacancies, the *less* is the rate of growth of the compound layer in the diffusion couple at the expense of diffusion of that component, *i.e.* the *less* is a value of the diffusional constant, k_1.

From a chemical viewpoint, this conclusion appears to be quite understandable because unoccupied (empty) sites (vacancies) present initially can hardly take part in chemical reactions yielding their products. It is just available atoms, ions, molecules or radicals and not native vacancies that are responsible for the progress of any interfacial chemical reaction. The formation of any reaction product is a result of their joint efforts.

In the case of the reaction-diffusion process, it does not seem substantiated to make a relatively small amount of missing atoms, say one atom in every hundred atoms, responsible for its course and to consider a much greater amount of available atoms (99) as an inert mass. The actual role of this single missing atom can roughly be estimated as 100% with the plus sign in the self-diffusion process and as 1% with the minus sign in the reaction-diffusion one.

Thus, the layer of any chemical compound must generally be considered to grow at the expense of stoichiometry of that compound. Boride layers are no exception. For any compound layer to occur between initial substances capable of reacting chemically, it does not matter, whether or not the compound under investigation has any range of homogeneity, structure deficiency, native vacancies or other imperfections [37-40].

Growth kinetics of boride layers at the diffusional stage of their formation, most frequently observed in practice, are somewhat more complicated than merely parabolic and can alternatively and more exactly be described by a system of two differential equations

$$\frac{\mathrm{d}x}{\mathrm{d}t} = \frac{k_{\mathrm{B}}}{x} - \frac{rg}{p}\frac{k_{\mathrm{Fe}}}{y} \qquad (10_1)$$

$$\frac{\mathrm{d}y}{\mathrm{d}t} = \frac{k_{\mathrm{Fe}}}{y} - \frac{q}{sg}\frac{k_{\mathrm{B}}}{x} \qquad (10_2)$$

where x is the outer FeB layer thickness, y is the inner Fe_2B layer thickness, k_B is the FeB layer growth-rate constant, k_{Fe} is the Fe_2B layer growth-rate constantPlots of layer thickness (left) and squared layer thickness (right) against time for boride layers formed between a Fe–30% Cr alloy and boron at a temperature of 850–950°C are presented in Fig. 20 as an example. The results of calculations for this alloy using a parabolic equation and the system of equations (10) are provided in Table 7. Average values of layer growth-rate constants for Fe–Cr alloys (10–30% Cr) and a 13% steel are summarized in Table 8.

With a 25% Cr steel, kinetic data were treated using only parabolic equations and the values of the total thickness of both layers because the thickness of each of them could hardly be measured separately with a sufficient accuracy due to their extreme irregularity. In this case, the value of the diffusional constant k_1 was found to be 0.72×10^{-14} m^2 s^{-1} at 850°C, 1.36×10^{-14} m^2 s^{-1} at 900°C and 2.40×10^{-14} m^2 s^{-1} at 950°C. These constants can be employed to estimate the boride layer thickness at intermediate values of time.

Values of the derivatives dx/dt and dy/dt entering into the system of equations (10) were found from the experimental layer thickness-time dependences by the numerical three-point method using a conventional computer program (linear approximation). To find a derivative for a given experimental point, (x_i, t_i), like those on left-hand plots of Fig. 20, data for its two neighboring points, (x_{i-1}, t_{i-1}) and (x_{i+1}, t_{i+1}), including the point $x_0 = 0$ at $t_0 = 0$, were used. Left-hand and right-hand derivatives, $(x_i - x_{i-1})/(t_i - t_{i-1})$ and $(x_{i+1} - x_i)/(t_{i+1} - t_i)$, were first found for this point and a mean value was then calculated. The derivatives could thus be found for all experimental points, excepting clearly the last one, for which a next neighbouring point is lacking.

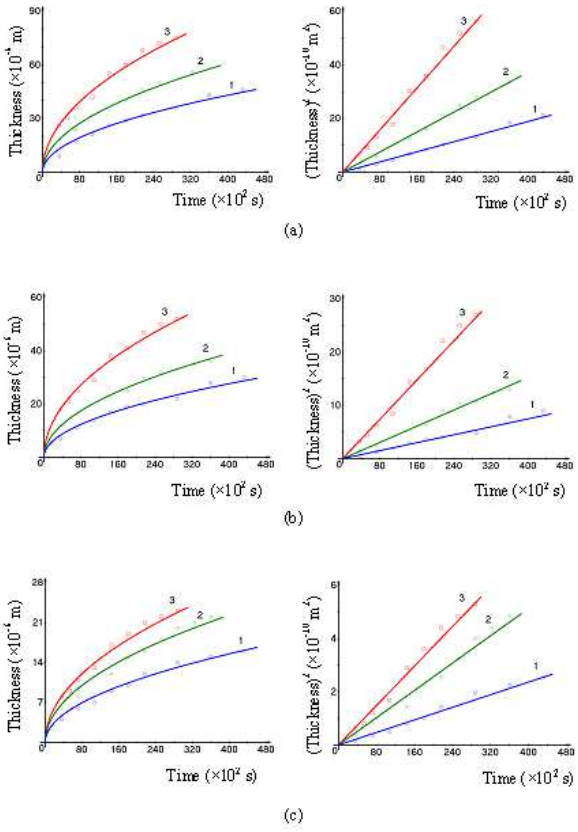

Fig. 20. Plots of layer thickness (left) and squared layer thickness (right) against time for (a) both boride layers, (b) the FeB layer and (c) the Fe_2B layer formed between a Fe–30% Cr alloy and boron at a temperature of 850°C (1), 900°C (2) and 950°C (3)

The results of calculations are strongly dependent upon a scatter of experimental points. To avoid this, preliminary approximation of the experimental data with any suitable analytical function is advisable. For example, the use of parabolic relations to approximate the layer thickness-time dependences and then to find the derivatives yields another set of values of k_B and k_{Fe} also provided in Table 8. Physically, k_B is the reaction-diffusion coefficient of boron atoms in the FeB layer, whereas k_{Fe} is the reaction-diffusion coefficient of iron atoms in the Fe_2B layer.

Comparing these with the average values of k_B and k_{Fe} found directly from the experimental points, it may be concluded

that both sets of the constants agree fairly well, providing evidence for the validity of the analytical treatment employed. Note that, in order to avoid a large computational uncertainty and to obtain acceptable results, the optimum number of experimental points must generally be nine or more.

The temperature dependence of layer growth-rate constants obtained is described in the 850–950°C range by a relation of the Arrhenius type $K = K_0 \exp(-E/RT)$, where K stands for any layer growth-rate constant, K_0 is the pre-exponential factor, E is the activation energy, R is the gas constant and T is the absolute temperature. A plot of ln K against T^{-1} for a Fe–30 % Cr alloy is shown in Fig. 21 as an example.

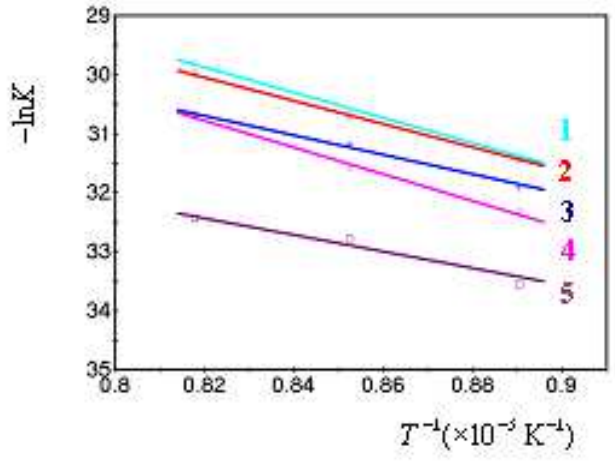

Fig. 21. Temperature dependence of the layer growth-rate constants, K, for a Fe–30% Cr alloy: 1 (×), kB from the system of equations (10); 2 (○), k1 from the equation x2 = 2k1t for both boride layers; 3 (+), kFe; 4 (◊) - k1 for the FeB layer; 5 (□) - k1 for the Fe2B layer.

Values of K0 and E found by the least-squares fit method are listed in Table 9. These are typical of diffusion-controlled processes [37-40, 47, 48] and can be used in practice to evaluate the values of growth-rate constants of boride layers at intermediate temperatures. In view of the rather limited number of Fe–Cr alloys investigated, it was hardly possible to establish any correlation between their chromium content and the value of the activation energy. For the total thickness of both boride layers formed on the surface of 25% Cr steel samples, the Arrhenius-type equation is k1 = 1.72×10–8 exp(–137.1 kJ mol–1/RT) m2 s–1.

3.4. Degradation of Boride Layers at Their Heat Treatment in the Absence of Boriding Media

Heat treatment of an as-received borided Fe–10%Cr alloy sample (Fig. 22a) in the absence of boriding media (a mixture of boron powder and KBF_4) results in a decrease of the thickness of the FeB layer and an appropriate increase of the thickness of the Fe_2B layer. As seen in Fig. 22b, 21600 s (6 h) reaction at 950°C causes the full disappearance of the FeB layer, about 90 μm thick initially. Further heat treatment of this sample leads to gradual disintegration of the Fe_2B layer into separate grains. As evidenced in Fig. 22c, grain-boundary diffusion appears to play a significant, if not decisive, role in this process.

Note that the FeB layer decomposes as a whole at the interface with the adjacent Fe_2B layer, with its compactness retaining and thickness decreasing, without any change in chemical composition. It is typical of compound layers with the microstructure of the fist type (a homogeneous phase without any homogeneity range) observed for Fe–Cr alloys (5–15% Cr) and a 13% steel.

Boride layers with the microstructure of the second type (two-phase) behave somewhat differently, as illustrated in Fig. 23 for a borided Fe–25% Cr alloy sample. As seen in Fig. 23b and c, the FeB layer, initially compact and around 40 μm thick, disintegrates into separate grains during the heat treatment of this sample in vacuum at 950°C, and after a 12 h reaction time disappears almost completely as a result of chemical reaction between iron and FeB to form Fe_2B.

This kind of consumption is characteristic of non-homogeneous layers. The first phase to disappear is seen in Fig. 23b and c to be (Fe,Cr)B because the remaining crystals of the outer (Fe,Cr)B–(Cr,Fe)B layer are blackish. This is confirmed by EPMA measurements. The chemical composition of blackish crystals of the outer (Fe,Cr)B–(Cr,Fe)B layer in Fig. 23c is 50 ± 2 at.% B, 17 ± 3 at.% Fe and 33 ± 4 at.% Cr. Wherever remained between blackish crystals, the more light (Fe,Cr)B phase has a composition of 50 ± 2 at.% B, 35 ± 3 at.% Fe and 15 ± 3 at.% Cr. Darker crystals of the inner $(Fe,Cr)_2B$–$(Cr,Fe)_2B$ layer have a composition of 33 ± 2 at.% B, 22 ± 5 at.% Fe and 45 ± 5 at.% Cr. Brighter crystals of this layer contain 33 ± 2 at.% B, 25 ± 3 at.% Cr and 42 ± 3 at.% Fe.

It should be noted that elongated crystals of the $(Cr,Fe)_2B$ phase penetrating deep into the alloy base actually do not grow in the absence of boriding media. The boron atoms released according to the reaction $2FeB = Fe_2B + B_{dif}$ at the interface between two boride layers, then diffuse across the Fe_2B layer and react with iron from the alloy base by the reaction $B_{dif} + 2Fe = Fe_2B$ to form more Fe_2B at the Fe_2B-alloy interface. The thinner the Fe_2B layer at a certain place, the shorter is the diffusion path and hence the higher is the supply of diffusing boron atoms to that place. Therefore, at thinner places the growth rate of the Fe_2B layer is higher than at thicker ones. As a result, the Fe_2B-alloy interface flattens with passing time, as evidenced in Fig. 23b and c.

Table 7. Thickness and growth-rate constants for boride layers formed at the Fe–30% Cr alloy–boron interface.

Temperature m(°C)	Time ($\times 10^2$ s)	Layer thickness ($\times 10^{-6}$ m)			k_1 ($\times 10^{-14}$ m^2 s^{-1})from the equation $x^2 = 2k_1t$			k ($\times 10^{-13}$ m^2 s^{-1}) from the system (10)	
		total	FeB	Fe_2B	total	FeB	Fe_2B	k_B	k_{Fe}
850	36	9	7	4	1.68	0.68	0.22	3.29	2.12
	72	17	11	6	2.00	0.84	0.25	3.41	2.13
	108	21	14	7	2.04	0.91	0.19	3.02	1.55
	144	26	17	9	2.34	1.00	0.28	3.20	1.78
	180	29	19	10	2.34	1.00	0.28	2.52	1.52
	216	32	20	12	2.37	0.93	0.33	2.10	1.55
	288	36	22	14	2.25	0.84	0.34	2.98	1.87
	360	43	28	15	2.57	1.09	0.21	3.56	1.79
	432	46	30	16	2.45	1.04	0.30	-	-
900	36	18	12	6	4.50	2.00	0.50	6.91	3.53
	72	24	16	8	4.00	1.78	0.44	4.91	2.71
	144	35	23	12	4.25	1.84	0.50	6.17	3.84
	180	40	25	15	4.44	1.74	0.52	6.50	4.07
	216	46	30	16	4.90	2.08	0.59	7.30	3.90
	252	50	32	18	4.96	2.03	0.64	4.25	2.73
	288	53	33	20	4.88	1.89	0.69	3.56	2.21
	324	56	35	21	4.83	1.89	0.68	3.49	2.03
	360	58	36	22	4,67	1.80	0.67	-	-
950	36	26	18	8	9.39	4.50	0.89	17.3	8.39
	54	30	21	9	8.33	4.08	0.75	9.53	3.89
	72	36	25	11	9.00	4.34	0.84	9.96	4.25
	108	42	29	13	8.17	3.89	0.78	13.3	6.04
	144	55	38	17	10.5	5.01	1.00	16.4	7.51
	180	60	41	19	10.0	4.67	1.00	12.9	6.03
	216	68	47	21	10.7	5.11	1.02	13.7	5.79
	252	72	50	22	10.2	4.96	0.96	7.75	3.13
	288	75	52	23	9.77	4.69	0.92	-	-

Table 8. Average values of layer growth-rate constants for Fe–Cr alloys (10–30% Cr) and a 13% steel.

Alloy or steel	Temperature (°C)	k_1 ($\times 10^{-14}$ m^2 s^{-1}) from the equation $x^2 = 2k_1t$			k ($\times 10^{-14}$ m^2 s^{-1}) from the system of equations (10) using experimental points		k ($\times 10^{-14}$ m^2 s^{-1}) from the system of equations (10) using approximated thickness-time dependences	
		total	FeB	Fe_2B	k_B	k_{Fe}	k_B	k_{Fe}
10 % Cr	850	19.8	4.1	5.9	16.4	22.7	14.0	19.9
alloy	900	30.4	6.6	8.6	25.2	33.1	22.2	29.6
	950	72.4	15.4	21.4	61.4	83.7	52.4	72.6
15 % Cr	850	13.1	2.9	3.6	11.3	14.5	9.64	12.5
alloy	900	20.6	4.6	5.9	14.7	18.3	15.4	20.4
	950	35.3	7.2	10.6	22.4	30.9	24.8	35.6
25 % Cr	850	5.3	1.6	1.1	5.45	5.21	4.77	4.38
alloy	900	8.9	3.1	1.7	9.76	7.88	8.92	7.18
	950	16.0	5.0	3.1	14.6	12.9	14.7	12.7
30 % Cr	850	2.23	0.93	0.27	3.01	1.79	2.45	1.37
alloy	900	4.60	1.90	0.58	5.39	3.13	5.04	2.89
	950	9.56	4.58	0.82	11.2	5.00	11.4	4.84
13 % Cr	850	8.8	1.6	3.0	7.35	12.2	5.81	9.60
steel	900	17.3	3.5	5.3	15.4	22.2	12.1	17.7
	950	28.1	5.9	8.3	19.6	27.6	20.1	28.1

Table 9. Values of K0 and E of a relation of the Arrhenius type K = K0 exp(–E/RT) describing the temperature dependence of growth-rate constants of boride layers (K0 in m2 s–1, E in kJ mol–1).

Alloy or steel	k_1						k_B		k_{Fe}	
	Total		FeB		Fe_2B					
	K_0	E	K_0	E	K_0	E	K_0	E	K_0	E
10% Cr alloy	12.8×10^{-7}	147.2	3.78×10^{-7}	150.5	3.34×10^{-7}	146.1	12.2×10^{-7}	149.9	12.3×10^{-7}	146.8
15% Cr alloy	2.32×10^{-8}	113.0	1.95×10^{-9}	103.8	1.88×10^{-8}	123.1	1.00×10^{-8}	107.9	4.38×10^{-8}	119.4
25% Cr alloy	3.78×10^{-8}	126.0	1.91×10^{-8}	130.5	3.27×10^{-9}	118.0	4.70×10^{-8}	128.8	1.90×10^{-8}	121.4
30% Cr alloy	1.18×10^{-8}	166.2	2.53×10^{-8}	181.7	2.48×10^{-9}	127.7	3.42×10^{-8}	175.4	7.45×10^{-9}	144.6
13% Cr steel	1.37×10^{-8}	132.9	1.49×10^{-7}	149.5	7.90×10^{-9}	116.4	2.44×10^{-7}	142.2	5.09×10^{-8}	122.9

These experiments clearly show the essential, if not decisive, role of diffusion of a gaseous boron-containing phase, probably BF_3 [1, 29], in the course of boriding of Fe–Cr alloy and steel samples in a mixture of boron powder and KBF_4 under reduced pressure. Defects of a certain kind and probably some solid-state transformation in the alloy base, providing the paths of rapid diffusion for the gaseous boriding agent, are responsible for the deep penetration of the $(Cr,Fe)_2B$ crystals into the sample bulk. It can hardly be solely a result of peculiarities of the crystal structure of iron and chromium borides, as is usually explained [1]. The regular arrangement of the constituting phases in both boride layers provides evidence for an additional solid-state transformation. It may either take place simultaneously with the layer growth or precede or follow it. This transformation may be closely connected with the occurrence of hot cracks that boron (> 0.007%) is known to cause in steels at elevated temperatures [49].

3.5. Microhardness of Boride Phases

A plot of microhardness against distance across the reacting phases for a Fe–30% Cr alloy is shown in Fig. 24 as an example. Its numerical values for all alloys and steels investigated are presented in Table 10.

Microhardness was found to vary considerably within both boride layers, especially those with the second type of microstructure in view of their non-homogeneity. The difference in microhardness of near-boride and far-away regions of the alloys or steels was insignificant (around 0.2 GPa).

For steels, the values obtained are close to those reported in the literature [1]. Higher values for Fe–25% Cr and Fe–30 % Cr alloys compared to Fe–5% Cr, Fe–10% Cr and Fe–15 % Cr alloys are probably due to the difference in their microstructures, the two-phase microstructure being more rigid and therefore harder than the single-phase homogeneous one.

3.6. Dry abrasive Wear Resistance of Boride Layers

Boriding the alloy and steel tablets for dry abrasive wear resistance tests was carried out at 950oC for 21600 s (6 h). The data obtained for borided 13% Cr steel samples are presented in Table 11 as an example. Wear resistance values are seen to be greater for the middle part of the layers than for their borders with adjacent phases due to its more developed texture and more ordered microstructure.

Comparative data on the wear resistance of the outer boride layer for the alloys and steels investigated are provided in Table 12. Its values proved to increase disproportionately with increasing chromium content of the alloys and steels. Borided materials with the layers of type I microstructure consisting of a homogeneous solid solution of chromium in the FeB compound or in the Fe2B compound exhibit a rather moderate increase in wear resistance compared to their bases.

It is 5-15 times for a Fe–10% Cr alloy and 6-27 times for a 13% Cr steel. A much greater increase is observed if the boride layers with a microstructure of type II are formed. For a Fe–25% Cr alloy it varies from 150 to 350 times. Boride layers with a microstructure of type II are so wear resistant that it is impossible to reach not only the alloy or steel base but even the inner layer by carrying out a reasonable number of tests. For this reason, comparison of the wear resistance values in Table 12 is restricted to the data for the outer boride layers.

In boride layers with type II microstructure, the (Cr,Fe)B phase (thin platelets, less than 100 nm thick) forms a rigid framework filled with the (Fe,Cr)B phase. Such network-platelet morphology results in enhanced wear resistance of the outer boride layer. The same applies to the inner boride layer consisting of (Cr,Fe)2B platelets embedded into the (Fe,Cr)2B matrix.

Thus, in order to increase the wear resistance of any product or part made of an ordinary iron-base alloy or steel, it is advisable first to cover its surface, for example galvanically, with a Fe–Cr alloy containing 25±5% chromium. Then, it is borided under carefully controlled temperature-time conditions based on the available kinetic data to ensure the necessary thickness and quality of a boride coating. If too high, brittleness of the coating thus obtained may be lowered by its alloying with Al, Si and other elements.

4. Conclusions

Two boride layers occur at the interface of Fe–Cr alloys (5–30% Cr) and chromium steels (10 and 25% Cr) with boron in the temperature range of 850–950°C and reaction times up to 43200 s (12 h).

In the case of Fe–5% Cr, Fe–10% Cr and Fe–15% Cr alloys and a 13% Cr steel, the outer boride layer bordering the boriding agent consists of the (Fe,Cr)B phase, whereas the inner boride layer adjacent to the solid substrate consists of the $(Fe,Cr)_2B$ phase. Each layer is a homogeneous phase (microstructure of type I).

With Fe–5% Cr and Fe–10% Cr alloys, boriding during 3600 s results in the formation of a single $(Fe,Cr)_2B$ layer. The next (Fe,Cr)B layer occurs after the first-occurred $(Fe,Cr)_2B$ layer has reached, depending on the temperature, a thickness of 100-180 μm.

With other alloys and steels, a reaction time of 3600 s is sufficient for both boride layers (Fe,Cr)B and $(Fe,Cr)_2B$ to form.

Each of two boride layers formed on the surface of Fe–25% Cr and Fe–30% Cr alloys and a 25% Cr steel consists of two phases and has a regular network-platelet morphology. The outer boride layer comprises the (Fe,Cr)B and (Cr,Fe)B phases, while the inner consists of the $(Fe,Cr)_2B$ and $(Cr,Fe)_2B$ phases (microstructure of type II).

The characteristic feature of both layers is a pronounced texture, the strongest reflections being {002} and {020} for the FeB phase and {002} for the Fe_2B phase.

Mechanism of formation of the layers generally includes the counter-diffusion of boron and iron (chromium) atoms across their bulks followed by subsequent chemical transformations at layer interfaces.

Diffusional growth kinetics of boride layers are close to parabolic and can more adequately be described by a system of two non-linear differential equations.

Temperature dependence of layer growth-rate constants obeys a relation of the Arrhenius type. Values of the activation energy obtained are typical of diffusion-controlled solid-state chemical reactions.

Boride layers with the microstructure of the second type exhibit a much higher wear resistance than those with the microstructure of the first type, the difference being more than an order of magnitude.

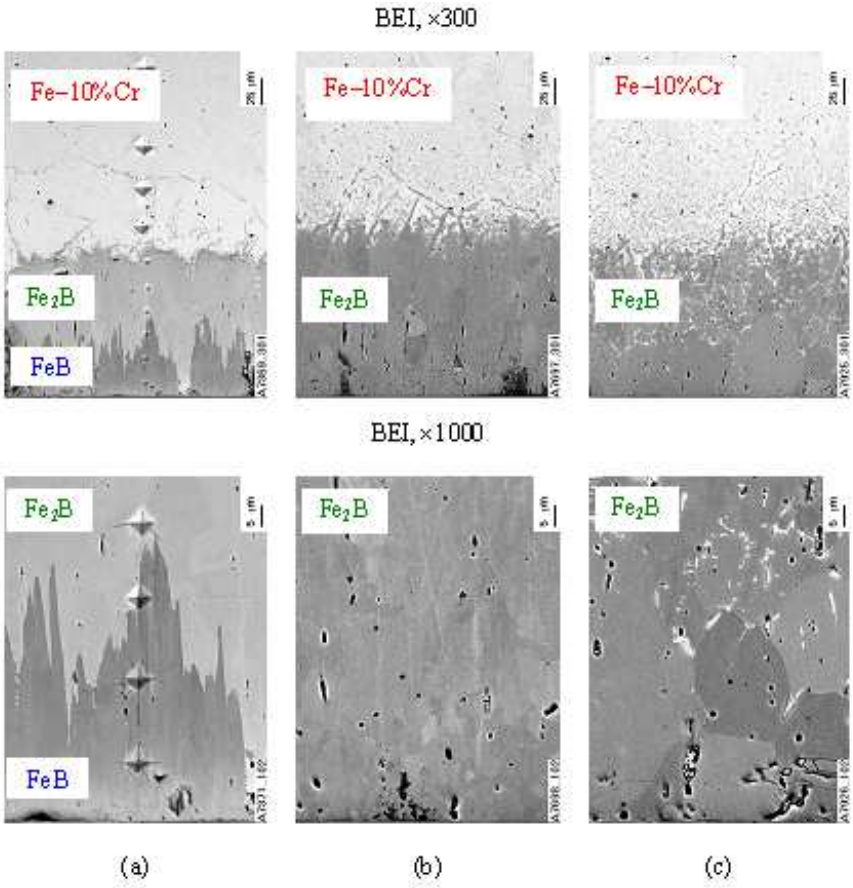

Fig. 22. Degradation of boride layers formed on the surface of a borided Fe–10% Cr alloy sample during its heat treatment in vacuum at a temperature of 950°C in the absence of boriding media: (a) as-received condition, (b) 21600 s (6 h) reaction time and (c) 43200 s (12 h) reaction time. BEI – backscattered electron image, magnification ×300 and ×1000.

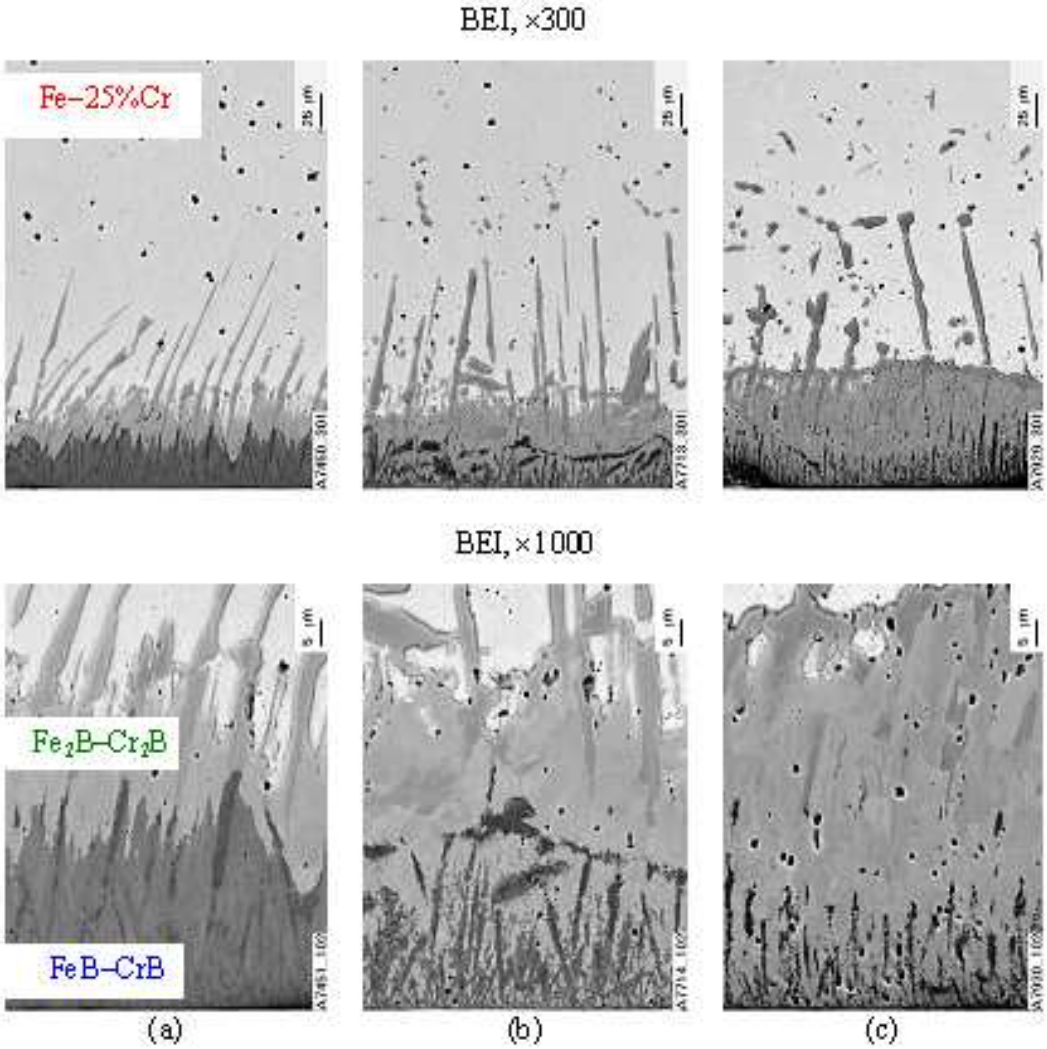

Fig. 23. Degradation of boride layers formed on the surface of a borided Fe–25%Cr alloy sample during its heat treatment in vacuum at a temperature of 950oC in the absence of boriding media: (a) as-received condition, (b) 21600 s (6 h) reaction time and (c) 43200 s (12 h) reaction time. BEI – backscattered electron image. Magnification: ×300 and ×1000.

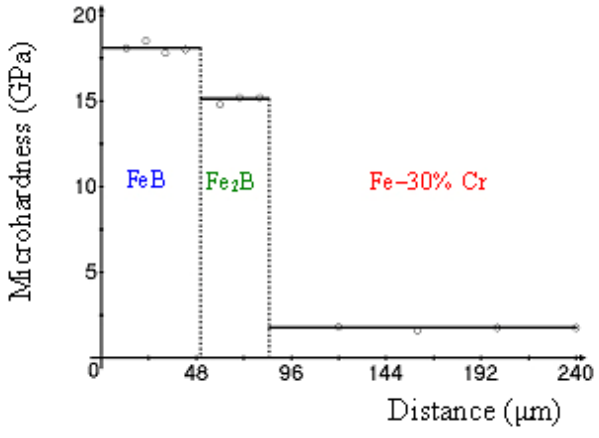

Fig. 24. A plot of microhardness against distance within reacting phases for a Fe–30% Cr alloy. Boriding conditions: temperature 950°C, reaction time 28800 s (8 h).

Table 10. Microhardness (GPa) of boride layers, iron-chromium alloys and steels

Alloy or steel	FeB	Fe_2B	Base
5% Cr alloy	15.6	13.0	0.87
10% Cr alloy	13.0	11.8	0.95
15% Cr alloy	17.4	14.4	1.30
25% Cr alloy	21.0	18.0	1.35
30% Cr alloy	19.1	16.2	1.75
13% Cr steel	17.9	16.1	5.9
25% Cr steel	17.8	15.9	1.70

Acknowledgements

The help of V.R. Sidorko, V.G. Khoruzha, L.V. Goncharuk, A.V. Samelyuk, V.V. Berezutsky, S.V. Bykova, L.A. Duma,

I.G. Kondratenko, K.A. Meleshevich, E.S. Rabotina, D.M. Pashko and V.M. Petukh with preliminary work, maintenance of equipment and carrying out experiments is acknowledged with sincere gratitude.

Table 11. Results of dry abrasive wear resistance tests of borided 13% Cr steel samples. Six consecutive tests were carried out on each of three borided samples until the steel base was reached. For comparison, one test was performed on a non-borided steel sample (n/b).

Borided sample number	Serial test number	Δm (g)	r	Δh (mm)	Phase
1	1	0.03035	11.0	0.035	(Fe,Cr)B
	2	0.01245	26.7	0.020	(Fe,Cr)B
	3	0.02140	15.6	0.030	(Fe,Cr)B
	4	0.02195	15.2	0.035	(Fe,Cr)B–$(Fe,Cr)_2B$
	5	0.03360	9.9	0.040	(Fe,Cr)B–$(Fe,Cr)_2B$
	6	0.05400	6.2	0.050	$(Fe,Cr)_2B$
2	1	0.03210	10.4	0.035	(Fe,Cr)B
	2	0.01315	25.3	0.020	(Fe,Cr)B
	3	0.02140	15.6	0.030	(Fe,Cr)B
	4	0.02195	15.2	0.035	(Fe,Cr)B–$(Fe,Cr)_2B$
	5	0.03165	10.5	0.040	(Fe,Cr)B–$(Fe,Cr)_2B$
	6	0.04385	7.6	0.050	$(Fe,Cr)_2B$
3	1	0.02315	14.4	0.025	(Fe,Cr)B
	2	0.01310	25.4	0.020	(Fe,Cr)B
	3	0.01290	25.8	0.020	(Fe,Cr)B
	4	0.01960	17.0	0.030	(Fe,Cr)B–$(Fe,Cr)_2B$
	5	0.03165	10.5	0.040	(Fe,Cr)B–$(Fe,Cr)_2B$
	6	0.05405	6.2	0.050	$(Fe,Cr)_2B$
n/b	1	0.3329	1	0.40	13% Cr steel

Note: Δm and Δh are changes in mass and height, respectively, of a sample; r is an increase in wear resistance in comparison with the steel base.

Table 12. Comparison of wear resistance values of the outer FeB layer for the alloy and steel samples investigated.

Alloy or steel	5% Cr alloy	10% Cr alloy	13% Cr steel	15% Cr alloy	25% Cr steel	25% Cr alloy	30% Cr alloy
	Microstructure of type I				Microstructure of type II		
Δm_{base} (g)	0.42335	0.32130	0.24335	0.31060	0.25730	0.29910	0.27740
Δh_{base} (mm)	0.47	0.43	0.30	0.41	0.31	0.38	0.37
r_1	1	1.32	1.74	1.36	1.65	1.42	1.53
$\Delta m_{boride\ layer}$ (g)	0.03853	0.02875	0.02645	0.00695	0.00100	0.00095	0.00090
$\Delta h_{boride\ layer}$ (mm)	0.040	0.035	0.030	0.010	~.0.003	~0.003	~0.003
r_2	11.0	11.2	9.2	44.7	257.3	314.8	308.5
r_3	1	1.34	1.46	5.54	38.5	40.6	42.8

Note: Δm and Δh are changes in mass and height, respectively, of a sample; $r_1 = \Delta m_{\text{base of a 5\% Cr alloy}} / \Delta m_{\text{base of a given material}}$; $r_2 = \Delta m_{\text{base of a given material}} / \Delta m_{\text{boride layer on a given material}}$; $r_3 = \Delta m_{\text{boride layer on a 5\% Cr alloy}} / \Delta m_{\text{boride layer on a given material}}$.

References

[1] L.G. Voroshnin, L.S. Lyakhovich: Boriding of Steel, Metallurgiya, Moskwa (1978), in Russian.

[2] A.G. Matuschka: Boronizing, Carl Hanser Verlag, Munchen (1980).

[3] A.K. Sinha: In A.K. Sinha (Ed.), Metals Handbook, ASM International, Metals Park, Ohio (1982) 844.

[4] H. Kunst, H. Schroll, R. Luetje, K. Wittel, E. Lugscheider, T. Weber, H.R. Eschnauer, C. Raub: in Ullmann's Encyclopedia of Industrial Chemistry, Vol. A16, Verlag Chemie, Weinheim (1991) 427.

[5] K. Holmberg, A. Matthews: Coatings Tribology, Elsevier, Amsterdam (2009).

[6] M. Hansen: Constitution of Binary Alloys, McGraw-Hill, New-York (1958).

[7] T.B. Massalski, J.L. Murray, L.H. Bennett, H. Baker: Binary Alloy Phase Diagrams, Vol. 1, American Society of Metals, Metals Park, Ohio (1986) 351.

[8] H. Okamoto: J. Phase Equil. Diffusion 25 (2004) 297.

[9] K. Genel, I. Ozbek, C. Bindal: Mater. Sci. Eng. A, 347 (2003) 311-314.

[10] I. Campos, J. Oseguera, U. Figueroa, J. A. García, O. Bautista, G. Kelemenis: Mater. Sci. Eng. A, 352 (2003) 261-265.

[11] M. Kulka, P. Pertek: Appl. Surf. Sci. 214 (2003) 278-288.

[12] C. Martini, G. Palombarini, M. Carbucicchio: J. Mater. Sci. 39 (2004) 933-937.

[13] E. Galvanetto, F. Borgioli, T. Bacci, G. Pradelli: Wear, 260 (2006) 825-831.

[14] S. Taktak: J. Mater. Sci. 41 (2006) 7590-7596.

[15] I. Campos, R. Rosas, U. Figuero, C. VillaVelázquez, A. Meneses, A. Guevara: Mater. Sci. Eng. A, 488 (2008) 562-568.

[16] X. Tian, Y. Lu, S.J. Sun, Z.G. Wang, W.Q. Hao, X.D. Zhu, Y.L. Yang: Mater. Sci. Techn. 24 (2008) 314-319.

[17] C.K.N. Oliveira, L.C. Casteletti, A. Lombardi Neto, G.E. Totten, S.C. Heck: Vacuum, 84 (2010) 792-796.

[18] J. Jiang, Y. Wang, Q. Zhong, Q. Zhou, L. Zhang: Surf. Coat. Techn. 206 (2011) 473-478.

[19] V.I Dybkov, W. Lengauer, K. Barmak: J. Alloys Compd. 398 (2005) 113-122.

[20] V.I. Dybkov, W. Lengauer, P. Gas: J. Mater. Sci. 41 (2006) 4948-4960.

[21] V.I Dybkov: Defect and Diffusion Forum 263 (2007)183-188.

[22] V.I Dybkov, L.V. Goncharuk, V.G. Khoruzha, K.A. Meleshevich, A.V. Samelyuk, V.R. Sidorko: Solid State Phenomena 138 (2008) 181-187.

[23] V.I. Dybkov: J. Mater. Sci. 42 (2007) 6614-6627.

[24] V.I. Dybkov, L.V. Goncharuk, V.G. Khoruzha, A.V. Samelyuk, V.R. Sidorko: Mater. Sci. Techn. 27 (2011) 1502-1512.

[25] V.I. Dybkov, V.R. Sidorko, V.G. Khoruzha, A.V. Samelyuk, L.V. Goncharuk: Poroshkovaya Metallurgiya (Powder Metallurgy, Ukraine) 7/8 (2011) 222-230.

[26] V.I. Dybkov, V.R. Sidorko, L.V. Goncharuk, V.G. Khoruzha, A.V. Samelyuk: Poroshkovaya Metallurgiya (Powder Metallurgy, Ukraine) 9/10 (2012) 24-37.

[27] V.I. Dybkov: Intern. J. Mater. Research 104 (2013) 617-629.

[28] V.I. Dybkov: Chemistry Journal 1(2015) 81-89.

[29] J. Brandstötter, W. Lengauer: J. Alloys Compd. 262-263 (1997) 390-396.

[30] L.I. Mirkin: Handbook on X-ray Analysis of Polycrystals, Fizmatgiz, Moskwa (1961) in Russian.

[31] S.S. Gorelik, L.N. Rastorguev, Yu.A.Skakov: X-ray and Electron-optical Analysis: Appendixes, Metallurgiya, Moskwa (1970) in Russian.

[32] V.A. Barinov, G.A. Dorofeev, L.V. Ovechkin, E.P. Elsukov, A.E. Ermakov: Phys. Status Solidi A, 123 (1991) 527-534.

[33] C. Gianoglio, C. Badini: J. Mater. Sci. 21(1986) 4331-4334.

[34] S. Okada, T. Atoda, I. Higashi: J. Solid State Chem. 68 (1987) 61-67.

[35] C. Gianoglio, G. Pradelli, M. Vallino: Metallurg. Sci. Techn. 1 (1983), 51-57.

[36] A. A. Bondar: In G. Effenberg, S. Ilyenko (Eds.), Landolt-Börnstein, Vol. 11D1, Springer, Berlin-Heidelberg (2007) 320-343.

[37] V.I. Dybkov: Reaction diffusion and solid state chemical kinetics, 1st ed., IPMS Publications, Kyiv (2002).

[38] V.I. Dybkov: Reaction diffusion and solid state chemical kinetics, 2nd ed., Trans Tech Publications, Zuerich (2010).

[39] V.I. Dybkov: Solid state reaction kinetics, IPMS Publications, Kyiv (2013). Free online version http://www.dybkov.kiev.ua.

[40] V.I. Dybkov: Chemical kinetics, IPMS Publications, Kyiv (2013). Free online version http://www.dybkov.kiev.ua.

[41] W. Seith: Diffusion in Metallen, Springer, Berlin (1955).

[42] K. Hauffe: Reaktionen in und an festen Stoffen, Springer, Berlin (1955).

[43] L.G. Yu, X.J. Chen, K.A. Khor, G. Sundararajan: Acta Mater. 53 (2005) 2361-2368.

[44] M. Keddam, S.M. Chentouf: Appl. Surf. Sci. 252 (2005) 393-399.

[45] M. Keddam: Intern. J. Mater. Research 100 (2009) 901-905.

[46] I. Campos-Silva, M. Ortiz-Dominguez, M. Keddam, N. Lapez-Prrusquia, A. Carmona-Vargas, M. Elias-Espinosa: Appl. Surf. Sci. 255 (2009) 9290-9295.

[47] H. Schmalzried: Chemical kinetics of solids, Verlag Chemie, Weinheim (1995).

[48] H. Mehrer: Diffusion in Solids: Fundamentals, Methods, Materials, Diffusion-Controlled Processes, 2nd ed., Springer, Berlin-Heidelberg (2010).

[49] G. V. Motovilin, M. A. Masino, O. M. Suvorov: Automobile Materials, Transport, Moskwa (1989), in Russian.